

GDP nowcasting with artificial neural networks: How much does long-term memory matter?

Kristóf Németh*, Dániel Hadházi†

March 1, 2024

Abstract

We apply artificial neural networks (ANNs) to nowcast quarterly GDP growth for the U.S. economy. Using the monthly FRED-MD database, we compare the nowcasting performance of five different ANN architectures: the multilayer perceptron (MLP), the one-dimensional convolutional neural network (1D CNN), the Elman recurrent neural network (RNN), the long short-term memory network (LSTM), and the gated recurrent unit (GRU). The empirical analysis presents results from two distinctively different evaluation periods. The first (2012:Q1 – 2019:Q4) is characterized by balanced economic growth, while the second (2012:Q1 – 2022:Q4) also includes periods of the COVID-19 recession. According to our results, longer input sequences result in more accurate nowcasts in periods of balanced economic growth. However, this effect ceases above a relatively low threshold value of around six quarters (eighteen months). During periods of economic turbulence (e.g., during the COVID-19 recession), longer input sequences do not help the models' predictive performance; instead, they seem to weaken their generalization capability. Combined results from the two evaluation periods indicate that architectural features enabling long-term memory do not result in more accurate nowcasts. Comparing network architectures, the 1D CNN has proved to be a highly suitable model for GDP nowcasting. The network has shown good nowcasting performance among the competitors during the first evaluation period and achieved the overall best accuracy during the second evaluation period. Consequently, first in the literature, we propose the application of the 1D CNN for economic nowcasting.

Keywords: GDP nowcasting, Artificial neural networks, 1D CNN, Long-term memory
Journal of Economic Literature (JEL) codes: C45, C51, C53

1 Introduction

Gross Domestic Product (GDP) is arguably the most important flow-type monetary measure of the economic activity of a country or region. GDP is often calculated on an annual basis, but in most advanced economies it is also measured on a quarterly frequency. Considering its relevance, the availability and reliability of these quarterly data are of great significance.

*Corresponding author. Faculty of Electrical Engineering and Informatics, BME, manzotta@gmail.com

†Department of Measurement and Information Systems, BME, hadhazi@mit.bme.hu

However, due to the time required for data collection and statistical data processing, statistical offices are delayed in releasing GDP data for the current quarter. The first measurements are usually available only a few months after the end of the current quarter, which makes it difficult to assess economic activity in real-time (i.e., synchronously). Therefore, many decision makers (such as central banks, budget offices, etc.) rely on the current quarter forecast, that is, the nowcast of GDP growth for more informed policy making. This underscores the need for accurate nowcasts.

In nowcasting current quarter GDP growth, one typically tries to extract the informational content of higher frequency monthly data to track the real-time development of economic activity. Such an analysis faces the following three problems (Giannone et al., 2008): (i) Combining monthly predictor variables and a quarterly target variable. (ii) Handling a large number of potential regressors. (iii) Monthly data are released at different times (unsynchronized) within a quarter. This leads to the so-called “*ragged edge*” problem, where some monthly features may have missing values, usually at the end of the sample period (Wallis, 1986).

In our study, we apply different artificial neural networks (ANNs) to nowcast the quarterly U.S. GDP growth of the current quarter. Using the monthly FRED-MD database, we measure the nowcasting performance of five different ANN architectures relative to a naive constant growth model: The multilayer perceptron (MLP), the one-dimensional convolutional neural network (1D CNN), the Elman recurrent neural network (RNN), the long short-term memory network (LSTM), and the gated recurrent unit (GRU). These architectures are similar in that they all try to meet the above-mentioned challenges of nowcasting. However, the models have a different structure. First, the MLP’s relatively simple architecture is not explicitly designed for sequence modeling. While we can form “training sequences” by hand and add them as input, the MLP does not recognize the temporal ordering in the data. This is not to say that the MLP cannot be used effectively in applications related to time series analysis, but in this regard, the MLP is the exception. Compared to the other ANNs investigated in this paper, the MLP is a simple, time-agnostic architecture, which is not tolerant to shifts (translations) in time (Ekman, 2021; Goodfellow et al., 2016). The 1D CNN and all other RNNs investigated in this paper are specifically designed for sequence modeling. They are capable of learning order dependence in sequential prediction problems. In other words, they are trained with *real* input sequences. Despite this similarity, even the 1D CNN and the RNNs differ substantially in how they handle the sequential data.¹ From the perspective of the empirical analysis, the question comes down to what architectural features are advantageous in terms of GDP nowcasting.

The first main contribution of this paper is that it proposes the utilization of a neural network architecture that has yet to be applied for economic nowcasting, namely the one-dimensional convolutional neural network (hereinafter, 1D CNN). Our results suggest that the 1D CNN could be a highly suitable architecture for GDP nowcasting as it generates accurate nowcasts for both of our evaluation periods, i.e., both during a balanced growth period and in times of high economic turbulence. While this ANN architecture has been neglected compared to the MLP and the more advanced gated RNNs, we would argue that it represents a “*sweet spot*” for

¹We will describe these differences in more detail in Section 3.

this type of analysis in many aspects. In contrast to the MLP, the 1D CNN has an intrinsic architectural constraint that usefully limits the hypothesis space, i.e., the range of mappings the network can learn during the training process. During training, the network learns the coefficients of different finite impulse response filters, so it can only learn a composition of time-invariant (translation-invariant) mappings. Intuitively, the network performs a series of hierarchical pattern recognition tasks where the result is time-invariant to the relative position of those patterns (Goodfellow et al., 2016). It is worth noting that the vast majority of the traditional time series approaches (e.g., the dynamic factor model) are also built around this assumption; namely, the conditional distribution of the target variable only depends on time through the regressors (predictors). From this point of view, it seems especially advantageous to narrow the hypothesis space to this type of mappings. Unlike the MLP, the 1D CNN is trained with input sequences, reflecting the architecture’s temporal “awareness”. Training of the 1D CNN is also helped by the perception of the temporal ordering in input data, ultimately leading to less trainable parameters (weights).

During the empirical analysis, we also investigate the nowcasting performance of three different recurrent neural networks (RNNs): The Elman RNN, also referred to as basic or “vanilla” RNN, and two types of its more advanced variants augmented with a so-called *gating* mechanism: the long short-term memory network (LSTM) and the gated recurrent unit (GRU). Similarly to the 1D CNN, RNNs can learn order dependence in input sequences and are restricted to learning time-invariant (translation-invariant) mappings between their inputs and outputs. However, compared to the 1D CNN, they handle sequential data in a more general, more complex way. Through their memory cells (basically, neurons forming a recurrent layer), they can learn a much wider range of time-invariant mappings rather than just a composition of finite impulse response filters. Hence, the hypothesis space of an RNN can be much larger than that of an 1D CNN containing the same number of parameters (weights).

The major novelty of gated RNNs is that they introduce a so-called *gating mechanism* (practically, element-wise multiplication) that enables the network to develop long-term memory. This feature helps to overcome the vanishing gradient problem of the vanilla RNNs, making them a much more viable option for modeling time series with path-dependent behavior, i.e., with long-term memory (Chung et al., 2014; Hochreiter & Schmidhuber, 1997). Financial time series, such as stock prices or even more foreign exchange rates, generally show characteristics of path dependency (e.g., a slowly decaying autocovariance function). Here, it can easily happen that the current value of the exchange rate is affected (supported) by a distant technical level whose effect, however, is no longer reflected in any nearby values. As a result, this old technical level should be remembered by the network in a predictive exercise. Since gated RNNs can learn those long-term dependencies between input and output, they can be highly effective in such predictive exercises. Formation of long-term memory comes at a cost, however: They contain much more trainable weights than an Elman RNN with the same number of neurons in their (hidden) state vector. Consequently, they usually need a large number of training samples to obtain a good level of generalization capability (Ekman, 2021; Goodfellow et al., 2016).

The second main contribution of the paper is that, first in the literature, it presents the

results of a comprehensive nowcasting *competition* between different ANN architectures. The competitor ANN architectures are then trained with different training configurations. These training configurations differ (i) in the length of the training sequences and (ii) in information sets available intra-quarterly. The nowcasting competition presented in this paper has three important aspects and purposes. First, it aims to identify the most suitable ANN architectures for GDP nowcasting. The second research question we try to answer is how important long-term memory is in GDP nowcasting. So, we investigate how the different competitor models' nowcasting performance changes with the length of the input sequences. Finally, we also try to measure how the nowcasting accuracy of the competitors changes with consecutive intra-quarterly data releases. So, we distinguish three different nowcasting scenarios depending on how many months of regressor data are available for the models within a given quarter. Accordingly, e.g., the 1-month nowcasting scenario refers to an information set that contains data for the monthly regressors until the first of a given quarter. We believe that the results of the empirical analysis might be indicative of some aspects of the underlying data-generating process. If, for example, the data-generating process of GDP growth was highly path-dependent (i.e., non-ergodic), then that would *likely* speak for the use of those gated RNNs with long input sequences.

We present the results from two evaluation (test) periods during the empirical analysis. While those evaluation periods overlap in time, they are very different in the characteristics of the target series, i.e., GDP growth. The first evaluation period ranges from 2012:Q1 to 2019:Q4, so it ends before the economic consequences of the COVID-19 pandemic hit the U.S. economy. The results for this period indicate that longer input sequences lead to more accurate nowcasts for the majority of the competitor models.

However, this effect ceases above a relatively low threshold value of around six quarters (eighteen months). While the MLP works best with 8 long sequences in every nowcasting scenario, other competitors yield better accuracy with 18 long input sequences in some nowcasting scenarios. While the 1D CNN produces its best (lowest) relative RMSE and MAE values with 18 long input sequences, the overall best accuracy in the first test period is achieved by the GRU trained with 8 long sequences. Both models beat the benchmark model in terms of nowcasting performance on a 5% significance level. Our second evaluation period is from 2012:Q1 to 2022:Q4, so it also includes periods of the COVID-19 crisis. Under such circumstances, shorter input sequences lead to more accurate nowcasts for all competitor models. In the second evaluation period, the best accuracy is achieved by the 1D CNN trained with 8 long sequences. We see that architectural complexity clearly hinders the gated RNNs' nowcasting performance in the second evaluation period. This time, they produce less accurate nowcasts than even the basic Elman RNN. Combined results from the two evaluation periods show that longer input sequences generally do not improve our models' predictive accuracy. That is especially interesting to see in the case of the LSTM and the GRU: While their architectural design enables them to handle long input sequences, forming a long-term memory, even these networks tend to have better accuracy with shorter sequences. Considering the results from the two test periods as a whole, architectural features supporting the learning of long-term dependencies do not play an important role in GDP nowcasting. Instead, they represent a comprising trade-off between

complexity and generalization capability for this specific predictive analysis.

The remainder of the paper is structured as follows: Section 2 briefly summarizes the related literature on the topic. Section 3 presents the different models applied in the empirical analysis, i.e., the five different neural network architectures mentioned above. Section 4 describes the data behind the analysis and exposes the nowcasting exercise. Then, it presents the results of the empirical analysis. Finally, Section 5 concludes.

2 Related works

Giannone et al. (2008) combine a dynamic factor model and the Kalman filter to nowcast the quarterly GDP growth for the US economy. Their two-step approach addresses all three problems of nowcasting mentioned before: it deals with the mixed frequency issue of combining monthly predictor variables and quarterly GDP, it can handle a large number of potential predictor variables, and it can cope with the ragged edge problem of the underlying data. Additionally, it has the potential to capture the essential dynamics of the time series of the panel.

After the seminal work of Giannone et al. (2008), DFMs have been found particularly successful at addressing many of the data issues inherent in nowcasting, and have been applied in many empirical studies (Stock & Watson, 2002). Matheson (2014) develop monthly indicators for tracking short-run trends in real GDP growth and conduct nowcasting analysis for 32 advanced and emerging-market economies. Marcellino and Schumacher (2010) conducts nowcasting analysis for the German economic activity, while Chernis and Sekkel (2017) perform a similar analysis for the Canadian GDP growth.

The fundamental idea of DFMs is that one or more latent factors dictates the movement of many different variables, each with an idiosyncratic component in relation to the factor(s). With historical data, the factor(s) can be estimated from the variables. Subsequently, even in future periods where not all data are complete, the factor(s) can still be estimated and used to generate forecasts for variables that are not yet published, as each variable's relation to the factor(s) has already been estimated. The theory behind the two-step estimator is derived in Doz et al. (2011).

Although ANNs have been the catalyst for numerous advances in various fields and disciplines in recent years, their impact on economics has been comparatively muted. While only a few study of nowcasting has applied ANNs, several other studies have applied neural networks to forecast macroeconomic and financial variables. For example, Tkacz (2001) uses neural networks to forecast the Canadian GDP growth rate between 1989 and 1992 by applying lagged GDP growth and several other financial variables, such as yield spreads and monetary aggregates. While Tkacz (2001) uses quarterly data to forecast Canadian GDP by using ANNs, Heravi et al. (2004) apply ANNs to forecast monthly industrial production between 1978 and 1995 for the three largest European economies, with data provided by Eurostat. In contrast to Tkacz (2001), they only use the information contained in the lagged values of monthly year-on-year growth of industrial production.

Besides these studies, ANNs have also been used in financial forecasting. For instance,

Kuan and Liu (1995) investigate the forecasting ability of ANNs and recurrent ANNs for daily exchange rates of five major currencies between 1980 and 1985. More recently, Torres and Qiu (2018) apply recurrent neural networks to daily data of several crypto-currencies, exchange rates, commodities and stocks between 2013 and 2017.

Results of Loermann and Maas (2019) indicate that the MLP outperforms the dynamic factor model in terms of now- and forecasting accuracy, while it generates at least as good now- and forecasts as the Survey of Professional Forecasters.

Compared to Loermann and Maas (2019), Hopp (2021) investigates a more complex recurrent network architecture, namely the long short-term memory network. The paper shows that LSTM networks produce more accurate nowcasts compared with DFMs on three different target series: global merchandise export values and volumes, and global services exports. In addition to better empirical performance for the three target series, LSTMs provide advantages over DFMs by being able to handle large numbers of features without computational bottlenecks and the ability to use any mixture of frequencies in features or target. Disadvantages include the stochastic nature of the parameter estimation and the lack of interpretability in their coefficients (Hopp, 2021). These advantages and disadvantages emerge at a more general level as well, in the comparison of the traditional time series approaches and the artificial neural networks (Goodfellow et al., 2016).

3 Models and methods

Artificial neural networks are flexible nonlinear estimators which represent the set of alternatives to the classical time series approaches. Similarly to most machine learning algorithms, ANNs can be used for classification problems, predictive exercises where the target variable is categorical, and also for regression function estimation. One of the biggest strengths of ANNs is that they can handle the curse of dimensionality in an *automated* way, much more naturally than traditional time series models. The latter set of models require the preparatory use of a dimension reduction method (e.g., PCA) or an unobserved component model for feature extraction, where the number of potential explanatory variables is large. For example, PCA can give us an optimal lower dimensional representation of the data in the sense that it changes the basis to the direction of maximum variance. However, we cannot be sure if there is no more relevant lower-dimensional representation of the features for the prediction of our target variable. Similarly, when we extract common factors from the input data, the procedure should be driven heavily by our a priori knowledge (choice): We should have a relatively concrete idea about the potentially relevant explanatory variables (features). After the set of observable indicators have been defined, method of explanatory factor analysis extracts common factors in such a way that they can explain the co-movements, i.e., the covariance structure of our features best. Here we see again that feature extraction is somewhat separated from the essential modeling task. Hence, it is not surprising that DFM-based GDP nowcasting is referred to as a two-staged estimation procedure in the literature (Giannone et al., 2008). By contrast, ANNs, can, in principle at least, learn the relevant feature representation by themselves.

The demand to connect the feature extraction with the actual predictive modeling task arises naturally and justifiably. Here is where artificial neural networks perform really well because they are inherently capable of learning the relevant representation of the features for the prediction of the target variable.²

This is not to say however, that ANNs are generally superior modeling frameworks compared to traditional linear models. While ANNs handle the *curse of dimensionality* more easily, they can perform worse in other areas. For example, they require a much more sophisticated data pre-processing step where we must deal with missing observations as well. One possible solution to fill up missing values is applying univariate ARMA(p,q) forecasts for each single input series. In this case, the lag lengths of the individual ARMA(p,q) models can be selected based on the value of Akaike or Schwarz information criterion (Greene, 2017; Loermann & Maas, 2019). Although missing data issue for ANNs can be solved in many ways, state space models handle this problem by design. If we think about the three big challenges of nowcasting mentioned in the introduction, we can say that mixed-frequency data can be treated relatively well in both modeling frameworks. Compared with the DFM, proper construction of our training and test samples with mixed-frequency data may require some additional effort.

More generally, we should also mention that even the smallest ANNs have much more parameters than a typical statistical model. The large number of trainable (*free*) parameters results in a relatively large hypothesis space. From the bias-variance trade-off follows that with a larger hypothesis space, it is more likely to find a hypothesis which fits the training data very well. This phenomenon is called overfitting, and it happens when a model learns the fine details and noise in the training data rather than the actual **systematic** relationship between the regressors and the target variable(s). Overfitting can substantially weaken a statistical model's generalization capability, and ANNs are substantially more prone to overfitting compared to the traditional time series models. So far, we tried to summarize the most important characteristics of ANNs as one of our nowcasting machines. In the following sections, we investigate those architectures in more detail that were adopted in the empirical analysis.

3.1 Multilayer perceptron

The multilayer perceptron (MLP), often referred to as fully connected neural network, is the straightforward extension of a single Rosenblatt perceptron.³ With non-linear activation (squashing) functions, the MLP can perform non-linear classification and regression tasks. It is one of the simplest types of a fully connected feedforward network.

²We should note that this kind of *connected* feature extraction (with some limitations) can also be conducted with classical time series approaches. However, ANNs have an advantage in representation learning.

³The Rosenblatt perceptron is a special type of neuron (just like the Adaline, for example), but hereafter, we will use the more generic name *neuron*

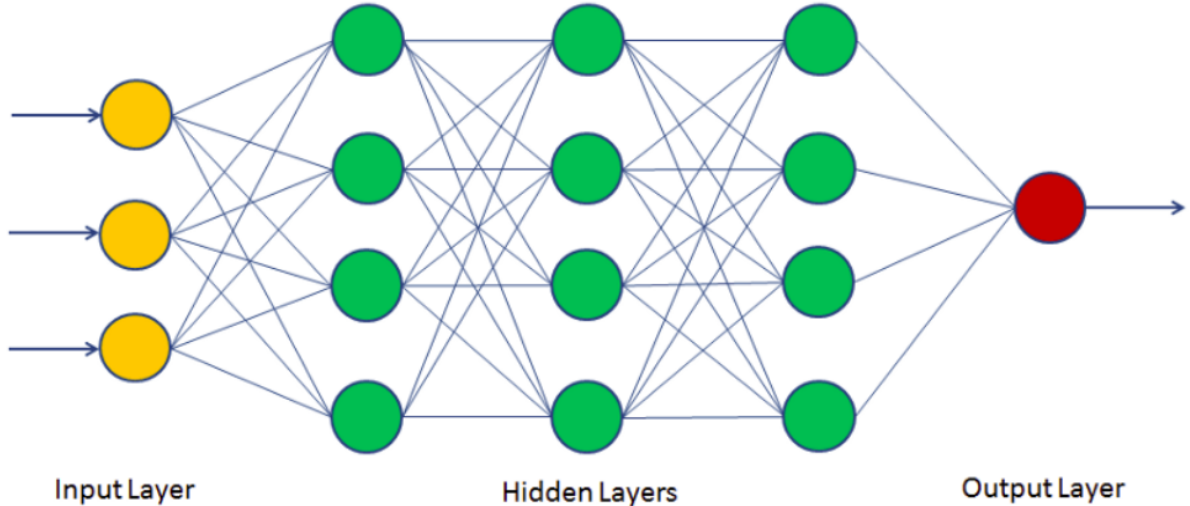


Figure 1: The architecture of the multilayer perceptron.

According to Figure 1, the MLP’s input-output mapping – if we assume the same non-linearity in each layer – is as follows:

$$\mathbf{y} = f \left(\mathbf{w}^l f \left(\mathbf{w}^{l-1} f \left(\mathbf{w}^{l-2} \dots f \left(\mathbf{w}^1 \mathbf{x} + \mathbf{b}^1 \right) + \mathbf{b}^{l-2} \right) + \mathbf{b}^{l-1} \right) + \mathbf{b}^l \right) \quad (1)$$

where \mathbf{w}^l is the matrix combining the weight vectors of the neurons in the l -th layer, \mathbf{b}^l is the bias vector in the l -th layer, and $f(\cdot)$ denotes the activation function (e.g., sigmoid) applied to the outputs of the neurons belonging to the same layer. An MLP, even in its simplest form when it contains one hidden layer, implements a non-linear mapping on its parameters. As Equation (1) suggests each hidden layer of an MLP can learn an arbitrary affine transformations of its inputs.⁴ As we will see below, this kind of universality will also affect the generalization capability of the network.

While MLPs can be used in time series forecasting, we should see that its architecture lacks any explicit temporal aspect. As long as any hidden layer can learn an arbitrary affine transformation of its inputs, the size of the hypothesis space can be even too large for our purposes. Notwithstanding that MLPs can learn time-invariant mappings between their inputs and outputs, their inner (hidden) structure is not invariant to shifts (translations) in time. A more fitting feedforward architecture for time series prediction can be the time-delay neural network, or in other words, the one-dimensional convolutional neural network (1D CNN).

3.2 1D Convolutional neural network

Convolutional neural networks (CNNs), similarly to MLPs, are also feedforward neural networks that typically consist of convolutional, pooling and fully connected layers. Without exaggeration, we can say that 2 dimensional CNNs have become the standard for various computer vision tasks in the last decade. As the field of application for 2D CNNs has constantly broadened,

⁴An affine transformation is the combination of a linear transformation with translations. Translation can be learned through the bias.)

1D CNNs have also received growing attention. 1D CNNs have recently achieved state-of-the-art performance levels in several applications related to time series analysis, such as biomedical data classification, anomaly detection, and structural health monitoring (Kiranyaz et al., 2021). We have not yet seen any application in the literature that is specifically related to economic nowcasting or forecasting. Nonetheless, in the following, we try to argue that GDP nowcasting might have exactly those characteristics that can render the 1D CNN a suitable competitor model.

In GDP nowcasting, we supposedly want to find a time-invariant mapping between our regressors (features) and our target variable. Intuitively, this means that the same regressor vector should have the same response in the target variable, even if it is shifted in time – assuming steady state. While MLPs can also learn time-invariant mappings, their architecture does not support this type of *restricted* learning by design. In contrast, 1D CNNs learn the coefficients of multiple finite impulse response filters in their convolutional layers. Consequently, the network is forced to learn a composition of time-invariant mappings in its convolutional layers. In other words, the network’s architecture intrinsically restricts the hypothesis space to the composition of time-invariant mappings, which we supposedly want to find in the nowcasting of GDP growth. Figure 2 below shows a simple example of single channel 1D convolution, where length of the input sequence is 7 and the length (size) of the convolution filter (kernel) is 3. According to the definition of the discrete convolution, the length of the resulting sequence is 5.

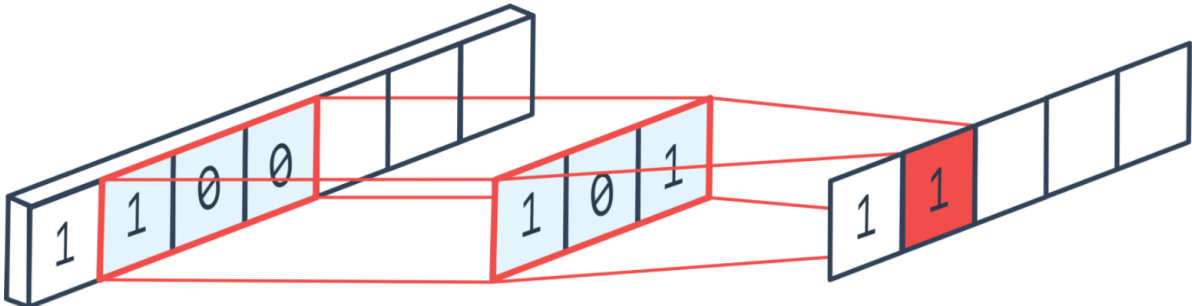


Figure 2: 1D convolution with a single input and output channel. Source: Ganesh (2019).

As Figure 2 suggests, a 1D CNN practically realizes finite impulse response filters on the input sequences, where filter coefficients (weights) are estimated during the training process. If we think about 1D CNN’s relation to traditional time series analysis, filtering is the first thing that should come into our minds. In traditional time series analysis, we often apply different frequency filters to reveal some hidden characteristics of the target series. For example, the Hodrick – Prescott filter is a popular frequency filter used to extract the unobserved trend and cycle components from a time series (Hodrick & Prescott, 1997). In terms of its characteristics, it is a low-pass pass filter, which attenuates the high-frequency components in the frequency spectrum of the target series. Naturally, we can think of any other frequency filter, whether low-pass, high-pass, or band-pass. While these filters are designed in the frequency domain, they are realized (applied) in the time domain. Knowing that multiplication in the frequency domain is equivalent to convolution in the time domain, we can see the 1D CNN’s strong

relation to the traditional filtering techniques. There is one major difference between them, however. When we apply a 1D CNN, we do not design our filters based on some a priori information or assumption, like higher frequencies should be associated with an unobserved cyclical component. Instead, we estimate the filter coefficients (weights) in part of the predictive analysis. By applying multiple finite impulse response filters, the network tries to create a representation of the input sequence(s) that is relevant to the prediction of the target variable. Since the filters within a convolutional layer are rather short, they typically pass high frequencies. Through the combination of multiple filters of the same or consecutive convolutional layers, the network can also learn input representations that would be associated with low-pass or band-pass filters.

Based on this simple example, we can also see that unlike MLPs, 1D CNNs are trained with sequential data where the network receives a fixed size input (training) sequence for each observation of the target variable. Obviously, in a more realistic setting we can have multiple input series (channels) and multiple convolution filters as well. In this case, we will have an output sequence (channel) for each convolving filter. Figure 3 below illustrates a case where we have 4 input channels (i.e., the input depth is 4), and we have 4 different convolution filters of length 5. Accordingly, we have 4 output channels (i.e., the output depth is 4). More generally, in a convolutional layer we will have a separate filter corresponding to each output channel of the feature map.

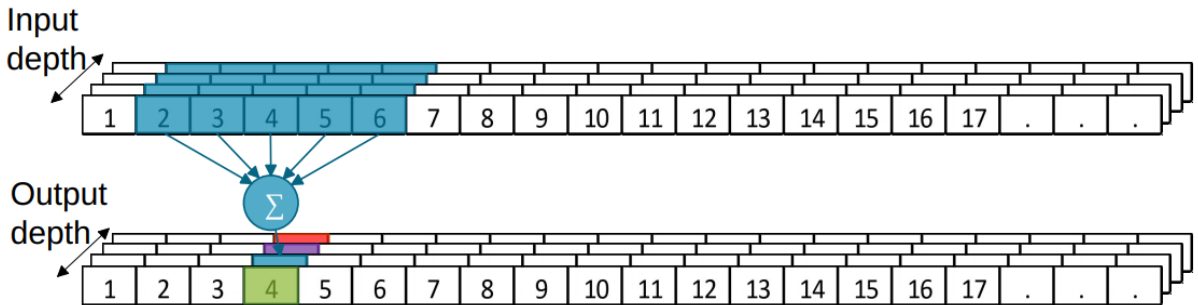


Figure 3: 1D convolution with multiple input and output channels.

As we have seen, a 1D convolutional layer applies an 1D convolution over an input sequence (signal) composed of several input channels (features or planes). In a more formal manner, the output vector (tensor) of the j -th output channel or feature map ($c_{out,j}$) in a 1D convolutional layer with input size (C_{in}, L_{in}) and output size (C_{out}, L_{out}) can be described as follows:

$$c_{out,j} = b_j + \sum_{i=0}^{C_{in}-1} f_{j,i} * c_{in,i} \quad (2)$$

where $f_{j,i}$ denotes the convolution filter corresponding to the j -th output channel (feature map) which slides over the i -th input channel. If k defines the filter size (length) within a convolution layer, $f_{j,i}$ can be represented by a $k \times 1$ row vector (1D tensor), containing k trainable weights (parameters). Continuing the interpretation of Equation (2), $*$ is the convolution operator⁵, C

⁵Rigorously speaking, it is the valid cross-correlation operator because filters (kernels) in a convolutional layer

denotes the number of channels, and L stands for the sequence length. From the definition of convolution (cross-correlation), it follows that $L_{out} = L_{in} - k + 1$.⁶

Based on Equation (2), in each 1D convolutional layer the networks learns the coefficients of different FIR filters. Not counting the biases, we will have $C_{out} \times C_{in} \times k$ trainable weights (parameters) in a given layer. Let us consider $f_{j,i}$ again, i.e., the convolution filter corresponding to the j -th output channel (feature map) which slides over the i -th input in channel. Since k defines the length of the convolution filters, it also controls how many terms of the input sequence are considered in the convolution while computing a single value in the output channel. Given a filter of size k , the possible time delays (d) are $d = 0, 1, \dots, k - 1$. Since the $f_{j,i}$ slides over the input sequence (series) in L_{out} steps, the following relationship will hold for every time delay d in every possible sliding step τ :

$$w_{j,i}(d) = \frac{\partial c_{out,j}(t)}{\partial c_{in,i}(t-d)} = \frac{\partial c_{out,j}(t-\tau)}{\partial c_{in,i}(t-d-\tau)} \quad (3)$$

where $c_{out,j}(t)$ stands for the value of the j -th output channel (feature map) in time t , and the corresponding time-related indices ranges as follows: $t = [0, 1 \dots (L_{out} - 1)]$, $d = [0, 1, \dots, k - 1]$, and $\tau = [0, 1, \dots, (L_{out} - 1 - t)]$.

Intuitively, Equation (3) shows that between given pairs of output and input channels (e.g., for a given (j, i) pair), the weights belonging to the same time delay (d) are the same. Consequently, we have locally shared weights within a convolutional layer (Ekman, 2021).⁷ By contrast, in the case of the MLP, Equation (3) obviously does not hold. As the MLP learns any arbitrary affine transformation within its hidden layers, it will also learn different weights for the same time delay. More precisely, it has no architectural restriction that would guarantee to learn shared weights for the same delay (shift) in time. While theoretically possible for the MLP to learn the same mapping as a given 1D CNN, that would require many more weights to train. It is worth noting that weight sharing has a potential drawback as well. With locally shared weights, the 1D CNN is restricted to learn only time-invariant mappings within its convolutional layers. The results of the empirical analysis will indicate whether that is really a drawback or not in this application.

3.3 Recurrent neural networks

This section presents the other three ANN architectures investigated in the empirical analysis: the Elman recurrent neural network, the long short-term memory network (LSTM), and the gated recurrent unit (GRU). As opposed to the unidirectional relationship between inputs and outputs, previously seen in feedforward networks (MLP, 1D CNN), recurrent neural networks (RNNs) introduce a feedback loop, where layer outputs can be fed back into the network (Dematos et al., 1996). Those neurons that create a cycle in the computational graph allow the network to exhibit dynamic behavior. They form the network’s internal (hidden) state or,

are not reversed.

⁶This is only true, if we assume the default values for the stride, padding and dilatation parameters. The more general formula can be found at: <https://pytorch.org/docs/stable/generated/torch.nn.Conv1d.html>

⁷Based on this, it is not surprising that the 1D CNN is often called as Time delay neural network (TDNN).

more intuitively, its memory. This architecture makes RNNs well-suited to applications with a temporal aspect or flow, such as natural language processing, speech recognition, or, in our case, time series analysis. Figure 4 shows how a recurrent layer can be unrolled in time. We create a copy of the recurrent layer for each timestep in the input sequence. This way, we practically convert the recurrent layer into a number of feedforward layers (Ekman, 2021).

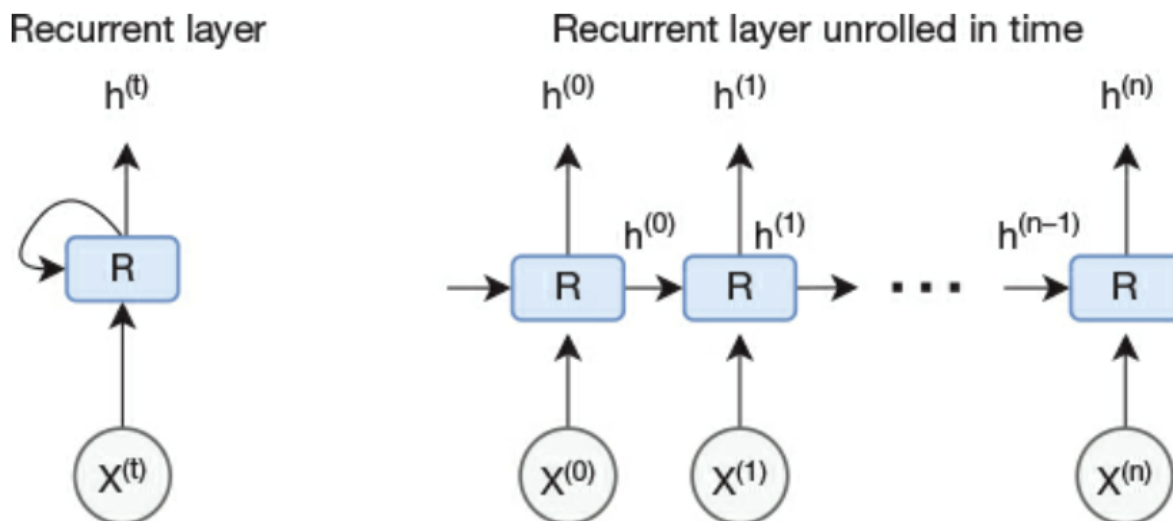


Figure 4: Recurrent layer drawn with one node representing an entire layer (left). Recurrent layer unrolled in time (right). Source: Ekman (2021) p. 247.

It should be emphasized that Figure 4 depicts a schematic representation of a recurrent layer, where the rectangular node, denoted by R , represents a full layer of recurrent neurons.⁸ Once we have the network unrolled in time, we can backpropagate the error in the same way as we do for a feedforward network. In cases with long input sequences, i.e, with many timesteps, it can be computationally more expensive though. This time, the backpropagation algorithm will produce one update value for each timestep, but when we later want to update the weight, there is only one weight to update. In other words, we have weight sharing between layers. The algorithm is known as *backpropagation through time* (BPTT). Werbos (1990) has written a detailed description about the algorithm, which also contains references to papers in which the algorithm was first used.

Similarly to the 1D convolutional layer, we also have weight sharing for the recurrent layer. This time, however, weight sharing does not work within a layer but between the consecutive layers of the unrolled network. As we have seen for the 1D CNN, weight sharing is beneficial because we have fewer weights to train. At the same time, the potential drawback of weight sharing is that the network is restricted to learning only a certain type of time-invariant mappings within its convolutional layers.⁹ As for the RNN, weight sharing provides a similar benefit of requiring fewer weights to train. Unfortunately, it surely has a negative implication this time,

⁸The number of recurrent neurons is often referred as hidden size in Deep learning frameworks, e.g., in Pytorch.

⁹Results of the empirical analysis will show, whether that is really a drawback or not in this application.

which is related to the operation of the BPTT algorithm.

In line with Figure 4, let us consider a simple case where a whole recurrent layer, represented by the rectangular node R, consists of a single neuron. Thus, we have a single weight for this recurrent neuron. What happens if this weight happens to be less than one, and we multiply it by itself as many times as many timesteps we have in the unrolled network (T)? It is easy to see that it will approach 0 (i.e., a vanishing gradient). Alternatively, in the other case, if the weight happens to be greater than one and we multiply it by itself T times, it will approach infinity (i.e., an exploding gradient). Not to mention that, the vanishing gradient problem described above is usually further worsened by saturated activation functions.

Due to vanishing gradients, RNNs tend to have a very “short” memory, limiting their usefulness in many applications (Ekman, 2021). Especially in those that require to learn long-term dependencies between inputs and outputs. Even with these considerations, we included one specific variant of the basic RNN in our nowcasting contest: the Elman network or Elman RNN. In an Elman network, each recurrent layer applies the following mapping for each element in the input sequence (Elman, 1990):

$$h_t = \tanh(x_t W_{i,h}^T + b_{i,h} + h_{t-1} W_{h,h}^T + b_{h,h}), \quad (4)$$

where h_t is the hidden state at time t , x_t is the input at time t , and h_{t-1} is the hidden state of the previous layer at time $t - 1$ or the initial hidden state at time 0. Based on the above, it is relatively easy to see that RNNs, similarly to 1D CNNs, will learn time-invariant mappings in their recurrent layers. Providing that the initialization of the hidden state is the same for all training sequences: e.g., h_0 consists of zeros.

After the short description of the Elman RNN, we present how to overcome the main limitations (vanishing gradients) associated with the basic RNN by using more advanced units when building the network. Introducing our last two competitor ANN architectures, we shift our focus on more advanced RNN variants that implement a so-called gating mechanism, namely the long short-term memory network and the gated recurrent unit (Chung et al., 2014; Hochreiter & Schmidhuber, 1997).

Long short-term memory (LSTM) network is a special form of gated RNNs which was introduced by Hochreiter and Schmidhuber (1997). A common way of drawing LSTM was introduced in a popular blog post that explains how LSTM works (Olah, 2015). Our summary on LSTMs is based on Ekman (2021), Goodfellow et al. (2016) and Olah (2015). Figure 5 below illustrates an LSTM layer unrolled in time for three timesteps. For each timestep t , the corresponding cell receives c_{t-1} and h_{t-1} from the previous timestep (cell) and x_t from the current timestep and outputs new values for the cell state (c) and the hidden state (h). Accordingly, h_t and c_t denote the *hidden state* (also referred to as the *output* of the LSTM cell) and the *cell state* (also known as the *internal state*) at time step t , respectively.

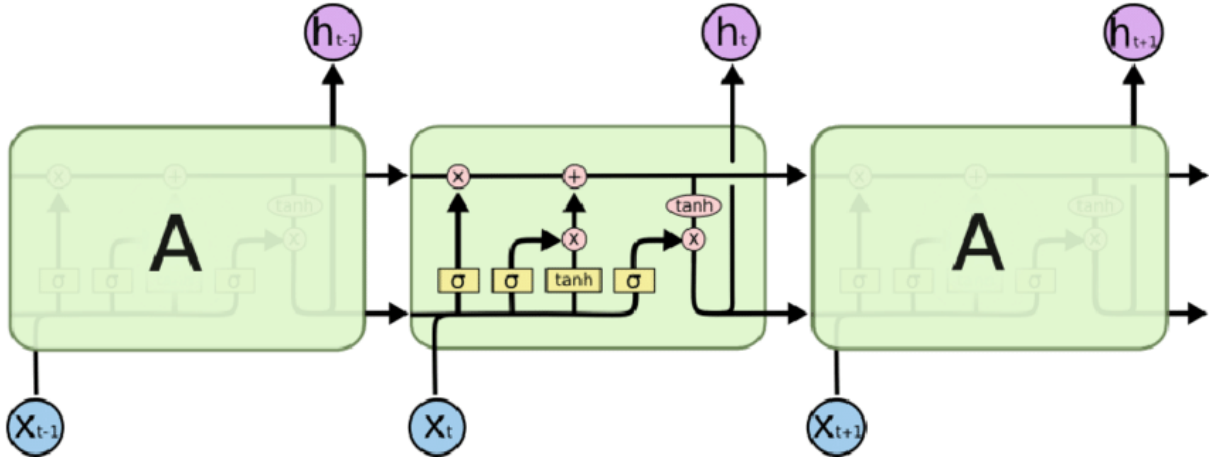


Figure 5: LSTM layer unrolled in time. Source: Olah (2015)

As Figure 5 illustrates, LSTM introduces a memory cell and three gates: an input gate, an output, and a forget gate. Essentially, the architecture then allows gradients to flow unchanged through the so-called *gradient highway*, mitigating the vanishing gradient problem of standard RNNs and rendering them more suitable for applications where long memory matters. Considering our empirical analysis, we are interested to see whether allowing for long memory does lead to better nowcasts.

Gated recurrent unit (hereafter, GRU) represents the other gated recurrent network adopted in our nowcasting analysis. Considering its architecture, GRU is very similar to an LSTM but belongs to a newer generation of gated RNNs (Chung et al., 2014). The GRU removes the cell state (denoted by c_t in the LSTM) and uses its hidden state (denoted by h_t , similar to the LSTM) even for transferring information. This way, it only has two gates, a reset gate and an update gate. Thereby, GRUs has fewer parameters and tensor operations compared to LSTMs (Chung et al., 2014). Consequently, they are a little speedier to train, and a bit less prone to overfitting. Researchers and engineers usually try both to determine which one works better for their specific use case. So we do the same in empirical analysis. Similarly to the 1D CNN, all the RNNs described above are trained with sequential data.

We have seen that gated RNNs provide a solution to the vanishing gradient problem through different realizations of the gating mechanism. This way, they can explore long-term dependencies in training sequences and connect information from the past to the present. Considering our empirical analysis, it is an essential question if there are such training sequences whose much older values have a significant impact on current-quarter GDP growth while that impact is no longer reflected in any more recent values of those sequences. To put this into a more formal manner, let us consider the conditional probability distribution of our target variable. Suppose that t denotes months and $q = 3t$ stands for quarters. In that case, the conditional probability distribution of quarterly GDP growth can be written as $\mathbb{P}(y_q|\Omega_t)$, where the information set Ω_t contains monthly regressor (indicator) series of length l with measurements available until the t -th month: $\Omega_t = [\mathbf{x}_t, \mathbf{x}_{t-1}, \dots, \mathbf{x}_{t-l+1}]$. If the series of quarterly GDP growth has no long-term

memory, i.e., it is ergodic, then Equation (5) is expected to hold for a given length of training sequences (l) and for all $t^* < t - l$ time period – at least with good approximation:

$$\mathbb{P}(y_t|\Omega_{t^*}, \Omega_t) = \mathbb{P}(y_t|\Omega_t), \quad (5)$$

This question is of essential relevance to our predictive analysis because the choice of the fitting neural network architecture largely depends on what we think about the data-generating process of GDP growth. In other words, in the context of system theory, what do we think about the impulse response function of the target variable? It is worth noting that both the MLP and the 1D CNN build around the assumption of fixed finite support for their target variable, in our case, GDP growth.¹⁰ While gated RNNs still assume a finite impulse response for the target variable, they allow for a much longer support. Furthermore, through their gating mechanism, they can dynamically adjust for the length of the impulse response. With this type of flexibility, however, comes complexity (much more trainable parameters) as well.

We should also note that gated RNNs are even more complex than those standard RNNs: While in standard RNNs cells are represented by a single neuron, LSTM and GRU cells contain several neurons inside, requiring at least a matrix for every gate. As a result, they are more prone to overfitting and highly sensitive to input noise. Moreover, due to their feedback loop, the stability analysis of (gated) RNNs is also more complicated than the feedforward networks. Even the initialization of such recurrent networks can be complicated in many cases (Ekman, 2021). On the other hand, if we think about the economy as a system with a long memory, then gated RNNs might provide more accurate nowcasts than any previously presented architectures, despite the aforementioned difficulties.

Next, in the empirical analysis, we let the data speak and evaluate the nowcasting accuracy of the different ANN architectures presented above. Accordingly, our competitor models will be the MLP, the 1D CNN, the Elman RNN, the LSTM, and the GRU. We believe that the results of this comprehensive nowcasting competition will identify the suitable architecture(s) for this predictive analysis and also reveal some aspects of the underlying data-generating-process of GDP growth.

4 Empirical analysis

In this section, we first describe the data used in the empirical analysis and the nowcasting exercise. After that, we present the results of the empirical analysis.

4.1 Data and feature selection

The target variable of the empirical analysis is the quarterly GDP growth, that is, the percentage change in the US Gross Domestic Product relative to the preceding period. The series is measured on a quarterly frequency and is available from 1947:Q2 to 2022:Q3. Thus it contains 302 observations. Figure 6 plots the time series for quarterly GDP growth.

¹⁰The support of a real-valued function $f(\cdot)$ is the subset of the function domain containing the elements which are not mapped to zero. In our case, finite support means that the impulse response is bounded in time.



Figure 6: U.S. Gross Domestic Product, percent change from preceding period (quarter). Source: Federal Reserve Economic Data (FRED).

When the empirical analysis was closed, the last GDP measurement was for 2022:Q4. In our empirical analysis, we try to extract the information content of several monthly macroeconomic indicators (i.e., features) whose intra-quarterly development might be related to current economic growth. The data for the input features comes from the FRED-MD database, the monthly database for Macroeconomic Research of the Federal Reserve Bank of St. Louis, which is described extensively in McCracken and Ng (2016).¹¹

The database consists of 134 monthly time series (indicators or features) which are clustered into eight categories:

1. Output and income (17 series)
2. Labour market (32 series)
3. Housing (10 series)
4. Consumption, orders and inventories (14 series)
5. Money and credit (14 series)
6. Interest and exchange rates (22 series)
7. Prices (21 series)
8. Stock market (4 series)

¹¹The FRED-MD database is available for download under the following link: <https://research.stlouisfed.org/econ/mccracken/fred-databases/>

The complete list of the data and the series-related data transformations are described in detail in Appendix A. Monthly indicator data are available from 1960:M1 to 2022:M12, so we have 756 observations for the potential regressors.

For the empirical analysis, all monthly indicators (features) are detrended using the corresponding data transformations. This is important because all of our competitor models, except for the MLP, are designed to estimate time-invariant prediction rules. Consequently, when both the target variable and the regressors (features) are stationary, we can generally expect better predictive performance from these models compared to when modeling non-stationary series.¹²

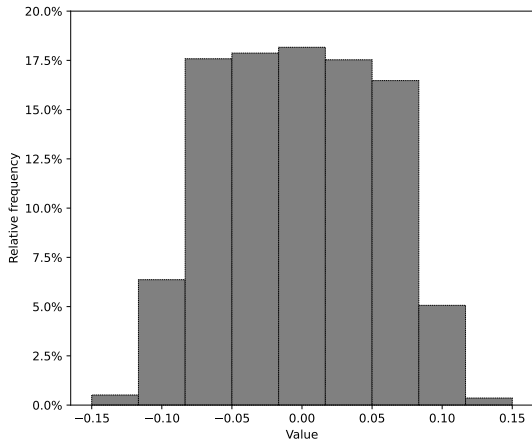
For the training of the different ANNs, we use all the monthly indicator series included in the FRED-MD database. At the same time, we introduce a bottleneck (encoder) layer, as the first layer in each network, to reduce the dimensionality of the feature space. The resulting low-dimensional embedding (state) vector contains a linear combination of the original variables, so in this respect, it performs a transformation on the data similar to principal component analysis (PCA). In the case of PCA, however, the weights of the resulting linear combination are determined to minimize the reconstruction error. By contrast, in the solution we propose, the weights of the linear combination are trained in the same integrated training process. Thus they are determined to minimize the prediction error. Considering the relatively small number of available training samples, this type of dimension reduction should significantly help each ANN’s generalization capability. Besides dimension reduction, we also apply regularization to the weight vector for the bottleneck layer (\mathbf{w}_b). Equation (6) describes the cost function augmented with the an L1 (Lasso) regularization term (Jiang et al., 2016):

$$C(\mathbf{w}) = \frac{1}{N} \sum_{i=1}^N L(y_i, f(\mathbf{w}, \mathbf{x}_i)) + \lambda \|\mathbf{w}_b\|_1 \quad (6)$$

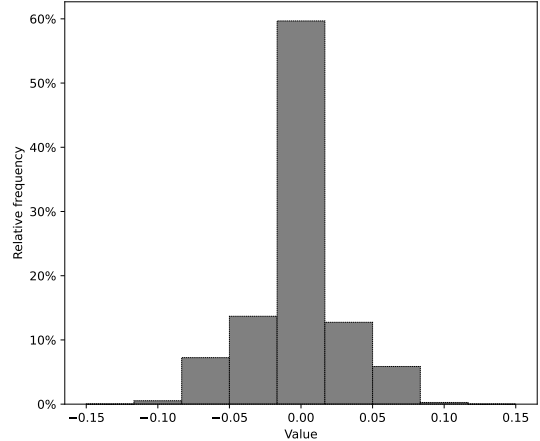
where $L()$ is the loss (criterion) function selected for training, $\|\mathbf{w}_b\|_1$ denotes the L1 norm of \mathbf{w}_b and λ is a hyperparameter which determines how severe the penalty is.¹³ Intuitively, a higher value of λ induces a bigger penalty to the L1 norm thus it leads to a more sparse weight vector. As Equation (6) suggests, we do not use regularization in any other layer of of the different networks. This L1 (Lasso) regularization leads to a sparse weight vector in the bottleneck (encoder) layer and ultimately results in feature selection (Jiang et al., 2016). Figure 7 below shows the histograms of the estimated parameters (weights and biases) for the bottleneck layer (\mathbf{w}_b^*) without regularization (7a) and with L1 regularization(7b).

¹²Figure A.1 below shows the level values of Real personal income (upper panel) and the result of the adequate data transformation (lower panel).

¹³We will specify the loss function in Section 4.2, during the description of the training process.



(a) Histogram of \mathbf{w}_b^* without regularization.



(b) Histogram of \mathbf{w}_b^* with L1 regularization.

Figure 7: Empirical distribution of the estimated parameters (weights and biases) for the bottleneck (encoder) layer in the 1D CNN. Source: Own editing based on FRED-MD.

Regarding its specification, the bottleneck layer is realized with a 1D convolutional layer. So the resulting tensor, in line with Equation 2, has a size of (C_{out}, L_{out}) . Since the MLP cannot be trained directly with sequential data, we flatten the resulting two-dimensional tensor (matrix) of the bottleneck layer. That is, we reshape it into a one-dimensional tensor (vector) of size $(C_{out} \times L_{out}, 1)$. This one-dimensional tensor will be added to the input layer of the MLP. Consequently, the MLP is the only competitor whose architecture changes with the length of the training sequences.¹⁴ In this sense, we can speak about training sequences (input sequences) in relation to the MLP as well. This simple modification allowed us to unify the training process for all competitor models.

4.2 The nowcasting exercise

Our full dataset ranges from 1960:Q1 to 2022:Q4, so that it contains feature observations for every month and target observations for every third month (i.e., for every quarter). We assume that quarterly GDP measurements are available for months M3, M6, M9, and M12.¹⁵

We evaluate the results from two test (evaluation) periods during the empirical analysis. The first evaluation period ranges from 2012:Q1 to 2019:Q4, so it ends before the COVID-19 pandemic would hit the US economy. It contains 32 observations for the quarterly GDP growth and 96 measurements for the monthly indicators. In comparison, the second evaluation period lasts until 2022:Q4, so it also includes those periods of the COVID crisis. Specifically,

¹⁴Actually, this is a necessity, which follows from the fact that the MLP does not recognize the temporal ordering in the data. Thus, longer training sequences must be associated with more neurons in its input layer.

¹⁵FRED data releases associate these quarterly measurements with timestamps M1, M4, M7, and M10. However, using these timestamps would be counter-intuitive in an empirical analysis focused on nowcasting. Following the literature, we assume that quarterly GDP measurements are published at the end of the current quarter. That corresponds with the reality since the first measurements (first estimates) are available about a month after the end of the current quarter.

it ranges from 2012:Q1 to 2022:Q4, containing 44 observations for the target variable and 132 measurements for the regressors.

In addition, we distinguish three different nowcasting scenarios depending on the information set available for our models. The *1-month* nowcasting scenario presumes that the monthly indicators' value is available up through the first month within a quarter. In the *2-month* scenario, the information set also contains feature observations released until the second month within the current quarter. Finally, in the *3-month* scenario, we use all monthly indicator data available at the end of the current quarter. If t denotes months and $q = 3t$ stands for quarters, then quarterly GDP growth can be denoted by y_q . In the followings, we define the nowcast (\hat{y}_q) as the conditional expected value of current-quarter GDP growth (Giannone et al., 2008):

$$\hat{y}_q = \mathbb{E}(y_q | \Omega_v, \mathcal{M}), \quad (7)$$

where Ω_v represents the information set containing monthly regressor (indicator) series of length l with measurements available until the v -th month. In line with the definitions of the different nowcasting scenarios, $v = [3t - 2, 3t - 1, 3t]$. Lastly, \mathcal{M} refers to the underlying model. Based on Equation (7), we see that the different nowcasting scenarios differ in their corresponding information sets. For example, $v = 3t - 1$ refers to the 2-month nowcasting scenario. Thus, within a given quarter, training sequences of length l include observations for monthly indicators until the second month. Intuitively, we expect to see the most accurate nowcasts in the 3-month nowcasting scenario ($v = 3t$), where all intra-quarterly indicator data are available for prediction. In Equation (7), \mathcal{M} denotes one of the competitor ANNs, i.e., $\mathcal{M} \in \{ \text{MLP, 1D CNN, RNN, LSTM, GRU} \}$. The underlying model determines what type of functions $f(\cdot)$, mapping the regressors into a predicted value for the target variable, can be learned during the training (estimation) process. Thus, the nowcast for quarter q is generated as follows:

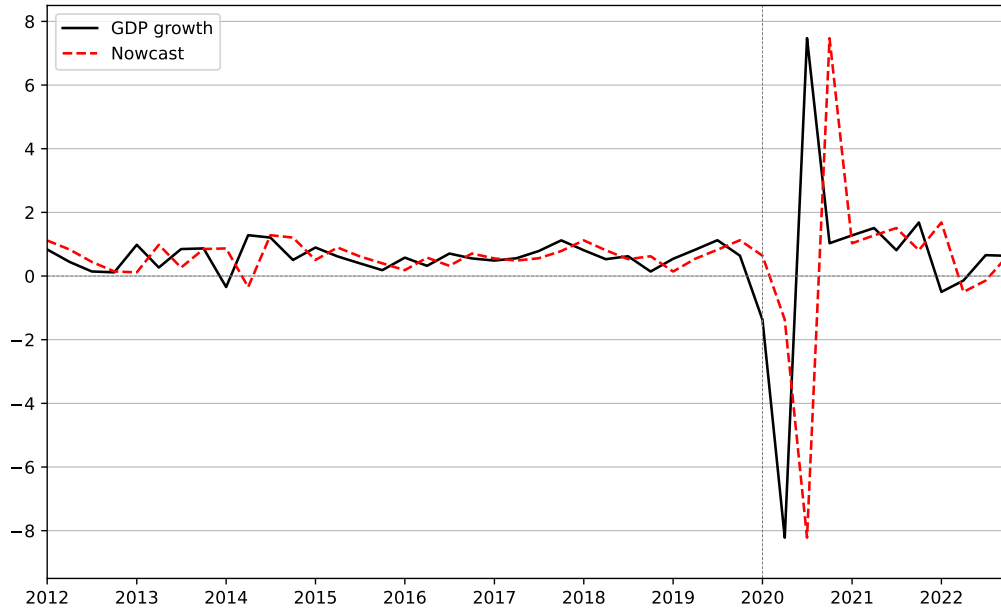
$$\hat{y}_q = f(\mathbf{x}_v, \mathbf{x}_{v-1}, \dots, \mathbf{x}_{v-l+1}) \quad (8)$$

where \mathbf{x}_v represents a row in the regressor vector, containing observations for n number of features in month v . As Equation (8) suggests, similarly to Giannone et al. (2008), we do not include any lagged values of the target variable in the regressor vector, which is denoted by $\varphi(\mathbf{x}_v)$. Hence, if l denotes the length of the training sequences (i.e. sequences of monthly indicators), the dimensionality of the regressor vector is $l \times n$. Accordingly, training sequences $(y_q, \varphi(\mathbf{x}_v))$ are formed by pairing the actual target observations for quarter q with the corresponding regressor vector. The training sequences are sampled then by a fixed-length rolling window where the size of the rolling window is determined by the sequence length (l). Since each (sub)sample of the features is related to a given quarterly target observation, successive rolling windows differ in values for their last 3 months. Consequently, they overlap in $l - 3$ monthly values, provided that $l > 3$.

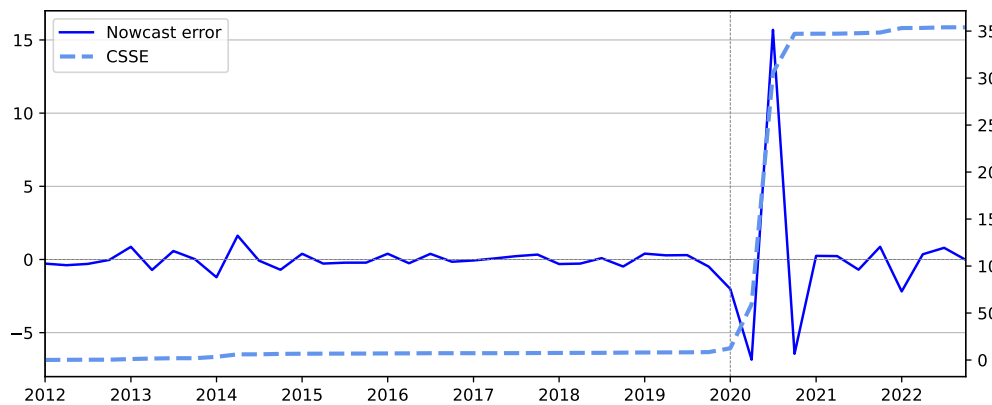
All of the competitor ANNs are estimated (trained) based on a rolling estimation (training) window, where the initial training window (set) ranges from 1960:Q1 to 2019:Q4. So, the size of the rolling window contains 200 training sequences: 200 observations for quarterly GDP growth (associated with months M3, M6, M9, M12) and 600 measurements for the monthly indicators

(i.e., regressors). The corresponding initial validation window (set) used for early stopping is from 2020:Q1 to 2021:Q4. Following the recommendation of the literature, we keep a small fraction of the data aside from training and use it for early stopping: 8 observations for the target variable and 24 for the explanatory variables (Amari et al., 1997). So, the first nowcast is generated for 2012:Q1, considering both evaluation periods. The number of increments between successive rolling estimation windows is 1 quarter (3 months). Based on (5), we generate then the series of nowcasts for the first evaluation period where $q \in \{2012:Q1, \dots, 2019:Q4\}$. We do the same for the second test period, where $q \in \{2012:Q1, \dots, 2022:Q4\}$. As the loss (criterion) function, we apply the mean squared error in line with the definition of the nowcast in Equation (7). When the final network is trained via the backpropagation algorithm, the resulting coefficients correspond to a local minimum of the loss function. Because there are multiple local minima, different random initializations of the backpropagation algorithm result in different weights and, therefore, different nowcasts. Kourentzes et al. (2014) suggests retraining the network for multiple random initializations, which results in a distribution of nowcasts. The mean of a kernel density estimate of the different nowcasts shows superiority in terms of nowcasting accuracy when compared to a single nowcast applying only one trained network. This so-called ensemble operator approach is also applied here for 30 different random initializations.

The predictive accuracy of the competitor models is evaluated relative to the naive benchmark model which assumes constant growth for GDP. From a computational point of view, this means that the nowcast for quarter q is assumed to be equal to its previous actual value: $\hat{y}_q = y_{q-1}$. While even this simple benchmark model might have good accuracy in some specific circumstances (see Figure 8), its predictive performance is expected to be generally weak, especially in periods of high economic turbulence. Figure 8 below, illustrates the predictive performance of the naive constant growth model during the two evaluation periods.



(a) The actual quarterly GDP growth (y_q) versus the nowcasts generated by the naive benchmark model ($\hat{y}_{b,q}$). The first evaluation period ranges from 2012:Q1 to 2019:Q4. The second evaluation period is from 2020:Q1 to 2022:Q4.



(b) Nowcast errors ($\hat{e}_{b,q} = y_q - \hat{y}_{b,q}$, left axis) and the cumulative sum of the squared nowcast errors (CSSE) for the benchmark model. The CSSE (right axis) is computed as $CSSE_b = \sum_q \hat{e}_{b,q}^2$, where $\hat{e}_{b,q}^2$ denotes the squared nowcast error of the benchmark model.

Figure 8: Nowcasting performance of the naive constant growth benchmark model. Source: Own editing based on FRED-MD.

Figure 8 shows that the naive benchmark model fits the data surprisingly well during the first evaluation period, i.e., in periods of quasi-stable economic growth. However, it fails when large shocks (positive or negative) hit the economy, as that is apparent during the second test period. The economic impact of the COVID-19 pandemic resulted in a V-shaped recession: a sharp downturn in 2020:Q2 followed by a quick rebound in 2020:Q3. While signs of the economic downturn could have been seen already in the macro indicators for April, the naive benchmark model clearly fails to predict the forthcoming recession in Q2. Following the assumption of

constant growth, it also misses the quick rebound in Q3, which affects its performance even worse. It is an interesting question: How accurately can our competitor models predict the V-shaped recession caused by the COVID-19 pandemic during the second evaluation period? We evaluate the nowcasting accuracy of our models in terms of relative root mean squared error (RMSE) and relative mean absolute error (MAE). As a benchmark, the constant growth model generates an RMSE of 0.513 and an MAE of 0.389 for the first test period. These measures for the second test period are 2.837 and 1.110, respectively. These values form the basis of the model evaluation, and also help to assess the absolute nowcasting accuracy of the competitor ANNs. Table 1 summarizes the above considerations and points out the strong negative relationship between the volatility of GDP growth and the nowcasting performance of the naive benchmark model.

Table 1: Main descriptive statistics of GDP growth and the nowcasting performance of the naive constant growth model in the two evaluation periods.

	1960:Q1 – 2022:Q4	2012:Q1 – 2019:Q4	2012:Q1 – 2022:Q4
\bar{y}_t	0.736	0.612	0.555
$\sigma(y_t)$	1.079	0.357	1.786
$100 \cdot (\sigma(y_t)/\bar{y}_t)$	146.554	58.312	321.667
RMSE	–	0.513	2.837
MAE	–	0.389	1.110
CSSE	–	8.424	354.016
CSSE / quarters	–	0.263	8.046

4.3 Results

In the following, we present the results of the empirical analysis. As the COVID-19 pandemic hit the US economy in 2020, we decided to evaluate our models on two different evaluation periods: The first evaluation period ranges from 2012:Q1 to 2019:Q4, so it does not reflect the economic impact of the COVID-19 pandemic. In comparison, the second evaluation period is from 2012:Q1 to 2022:Q4, containing those periods of the COVID crisis as well. We believe that the results from these two evaluation periods show a more balanced and well-rounded picture of the different models’ generalization capability. Clearly, these two test periods are very different in their characteristics. The first can be basically described as a period of balanced economic growth. Under such circumstances, the naive benchmark model is expected to be a strong contender for our competitor models. Consequently, competitor models should accurately predict even the more intricate movements in economic growth to beat the benchmark model. In contrast, the second evaluation period would favor the models that can capture the sharp V-shaped recovery of 2020:Q2 and 2020:Q3. We believe that results from these two evaluation periods will provide a robust assessment about the generalization capability of the different competitor models, showing their strengths and weaknesses.

Below, Table 2 presents the results of the nowcasting competition in our first evaluation

(test) period, which ranges from 2012:Q1 to 2019:Q4. We will see how the length of the training sequences affect the competitor models' nowcasting accuracy in the different nowcasting scenarios. Accordingly, Table 2 reports the results for four different lengths of training sequences: $l = [8, 18, 36, 48]$. We also investigated the nowcasting performance with longer sequences, but training sequences longer than 48 months did not yield more accurate nowcasts for any competitor model, neither in RMSE nor in MAE terms. This applies for both evaluation periods. In the inference phase, we use input sequences (i.e., test sequences) of the same length as we used by forming the training sequences in the training phase. Given that test sequences and training sequences are of the same length, we use the more generic term *input sequences* for both when describing the results.

Table 2: Nowcasting performance of the competitor models relative to a naive constant growth model for GDP: RMSE and MAE evaluation. Evaluation period: 2012:Q1 – 2019:Q4.

	$v = 3t - 2$		$v = 3t - 1$		$v = 3t$	
	RMSE	MAE	RMSE	MAE	RMSE	MAE
MLP ($l = 8$)	0.669*	0.761*	0.657*	0.707**	0.664*	0.706**
MLP ($l = 18$)	0.690*	0.758*	0.678*	0.733*	0.692*	0.748*
MLP ($l = 36$)	0.738*	0.778*	0.728*	0.767*	0.737*	0.775
MLP ($l = 48$)	0.755*	0.788*	0.741*	0.776*	0.755	0.782*
1D CNN ($l = 8$)	0.633**	0.687**	0.637**	0.725**	0.640**	0.720**
1D CNN ($l = 18$)	0.693*	0.749**	0.659*	0.728**	0.624**	0.687**
1D CNN ($l = 36$)	0.714*	0.754*	0.625**	0.693**	0.624**	0.694**
1D CNN ($l = 48$)	0.754*	0.786*	0.695*	0.750**	0.693*	0.764*
RNN ($l = 8$)	0.663*	0.742*	0.619**	0.683**	0.643*	0.671**
RNN ($l = 18$)	0.660*	0.731**	0.640**	0.690**	0.631**	0.634**
RNN ($l = 36$)	0.691*	0.759*	0.638**	0.684**	0.653**	0.648**
RNN ($l = 48$)	0.680*	0.745*	0.626**	0.661**	0.639**	0.638**
LSTM ($l = 8$)	0.662*	0.751*	0.613**	0.660**	0.653**	0.661**
LSTM ($l = 18$)	0.660*	0.738*	0.630**	0.680**	0.641**	0.659**
LSTM ($l = 36$)	0.669*	0.761*	0.643**	0.700**	0.669**	0.678**
LSTM ($l = 48$)	0.665*	0.751*	0.626**	0.667**	0.667**	0.662**
GRU ($l = 8$)	0.655**	0.740*	<u>0.562**</u>	0.619**	0.627**	0.648**
GRU ($l = 18$)	0.649**	0.732**	0.582**	0.628**	0.620**	<u>0.618**</u>
GRU ($l = 36$)	0.665*	0.738*	0.626**	0.683**	0.629**	0.622**
GRU ($l = 48$)	0.662*	0.729**	0.612**	0.652**	0.625**	0.633**

Notes: This table reports the relative RMSE and MAE of GDP growth for our competitor models relative to a naive constant growth model for GDP. A value below one indicates that the competitor model beats the naive benchmark model. The stars denote statistical significance at 10%(*), 5%(**) and 1%(***) level of the one-sided Diebold and Mariano (1995) test. Columns are related to the individual nowcasting scenarios: e.g. $v = 3t - 2$ refers to the 1-month nowcasting scenario. Within each nowcasting scenario, best (lowest) relative RMSE and MAE values are highlighted in bold for each competitor model. The overall best relative RMSE and MAE values are highlighted in bold and underlined.

Based on Table 2, it is apparent that all of the competitor models can beat the naive benchmark model in terms of nowcasting accuracy. With properly selected training configurations, i.e., with adequate combinations of the sequence length and the nowcasting scenario, each network architecture generates significantly more accurate nowcasts than the benchmark model. Recalling that the first evaluation period had been characterized by balanced and stable economic growth, the results of Table 2 seem to justify the use of these ANN architectures for economic

nowcasting.

Focusing on the nowcasting performance of the different ANN architectures, we see that the MLP generates the most accurate nowcasts with 8-month-long input sequences. The only exception is the 1-month nowcasting scenario, where 18 long input sequences yield slightly more accurate nowcasts in terms of MAE evaluation. However, the performance gain for the longer sequences is not significant and is eventually negligible (0.758 compared to 0.761). It is easy to see that different or more random initialization can easily flip this difference around. With 8-month-long input sequences, the MLP significantly outperforms the benchmark model on a 10% significance level in all nowcasting scenarios. Furthermore, it beats the constant growth model even on a 5% significance level in the 2-month and 3-month nowcasting scenarios regarding MAE evaluation. While the MLP performs well compared to the naive benchmark model, its (absolute) accuracy somewhat lags behind the other four ANN architectures explicitly designed for sequence modeling. It is also worth noting that longer input sequences yield gradually less accurate nowcasts for the MLP. With input sequences of length 36 and 48, there are training configurations where the MLP fails to beat the performance of the benchmark model in terms of statistical significance. While relative RMSE and MAE values are still below one, the performance gain is not uniformly significant in the 3-month nowcasting scenario. Results for the MLP in Table 2 indicate that the nowcasting accuracy of the MLP weakens with longer input sequences. We assume that the MLP’s performance is somewhat hindered by its simple time-agnostic architecture during the first evaluation period, where nowcasting performance largely depends on identifying the more subtle movements in economic activity.

Compared to the MLP, the 1D CNN generally produces more accurate nowcasts, especially in the 2-month and 3-month nowcasting scenarios. With proper length of input sequences, the 1D CNN beats the benchmark model across all nowcasting scenarios on a 5% significance level regarding both RMSE and MAE evaluation as well. Table 2 shows that the same can be said only about the GRU, the competitor with the overall best accuracy during the first evaluation period. The role of sequence length seems less clear than in the case of the MLP, however. Table 2 indicates that the most accurate nowcasts are generated with 18 long input sequences in the 3-month nowcasting scenario. In terms of statistical significance, the relative performance gain over the naive benchmark model does not improve with longer input sequences but becomes worse above 36 months. Table 2 also shows that the nowcasting accuracy of the 1D CNN gradually improves with consecutive intra-quarterly data releases. As we might have expected, the network generates the least accurate nowcasts in the 1-month nowcasting scenario. Still, it significantly beats the benchmark model in the 2-month and 3-month nowcasting scenarios for every sequence length setting. In general, the 1D CNN yields strong nowcasting performance across all the training configurations, beating the benchmark model on a 5% significance level regarding both RMSE and MAE evaluation.

Results in Table 2 indicate that the Elman (basic or “vanilla”) RNN reaches its full potential with 18 long input sequences. With input sequences this long, the basic RNN outperforms the naive benchmark model on a 5% level of significance in every nowcasting scenario. We should add that the performance advantage is significant only on a 10% level in terms of RMSE evaluation.

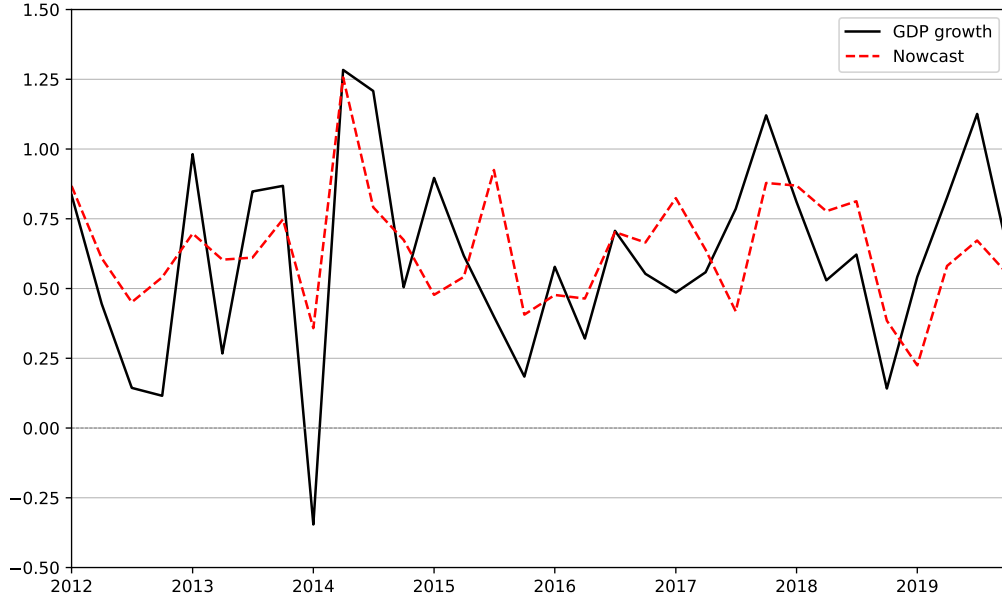
We also see that longer input sequences do not yield significantly more accurate nowcasts for the Elman RNN in any nowcasting scenarios. On the other hand, nowcasting accuracy does not become significantly worse either. As Table 2 shows, the LSTM has almost identical nowcasting performance as the basic RNN during the first evaluation period. With 8 long input sequences, in the 2-month nowcasting scenario, the LSTM produces a relative RMSE of 0.613 and a relative MAE of 0.660, beating the benchmark model on a 5% significance level in terms of RMSE and MAE evaluation. Accuracy slightly improves with 18 long sequences in the 1-month and 3-month nowcasting scenarios. Along with this, relative RMSE and MAE values are virtually the same as what we have seen for the basic RNN or the 1D CNN.

By comparison, results for the GRU show that our other gated RNN has an edge over the Elman network. Moreover, as Table 2 shows, the GRU generates the most accurate nowcasts during the first evaluation period. In terms of RMSE evaluation, the GRU performs best with only 8 long input sequences. The network yields an overall best relative RMSE of 0.562 and a relative MAE of 0.619 in the 2-month nowcasting scenario. Regarding the relative MAE values, a bit longer input sequences seem to improve the nowcasting accuracy. With 18 long sequences, the GRU generates a relative RMSE of 0.620 and an overall best relative MAE of 0.618 in the 3-month nowcasting scenario. While these results are the best for the first evaluation period, we should see that neither of these relative RMSE or MAE values indicate a performance advantage over the benchmark model, which would be significant on a 1% significance level. Results for the GRU and the relatively weak performance of the LSTM suggest that the performance advantage of the GRU is hardly due to architectural features supporting long-term memory. We would rather explain the results from the perspective of the bias-variance trade-off. From this point of view, the GRU seems to have just the right amount of free (trainable) parameters (weights) considering the characteristics of the first evaluation period. On the one hand, the GRU has three times more parameters than an Elman RNN with a same-sized hidden state. Having many more parameters means the model will have a much higher chance of fitting the training data well, i.e., with less bias. On the other hand, the GRU is a more efficient and parsimonious architecture than the LSTM, having only three-quarters as many parameters as an evenly sized LSTM. Since the first evaluation period is characterized by stable, balanced economic growth, fitting the training data well might be highly important. It is even more important than having a strong generalization capability. However, too many trainable parameters always lead to the excess variance of the estimator. From this point of view, it is not surprising that the characteristics of the first evaluation period favor those models with more trainable weights, the GRU in our case. Finally, the nowcasting performance of the gated RNNs does not worsen significantly with longer input sequences, but it does not improve either.

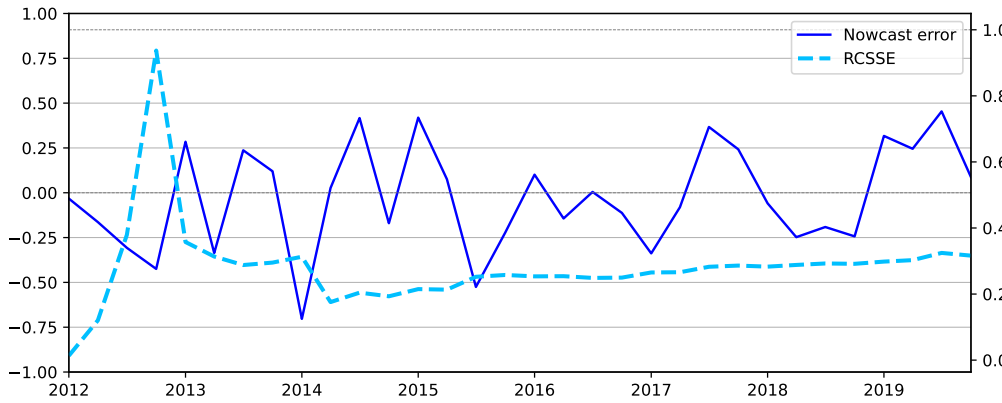
To summarize the results for the first evaluation period, we see that longer input sequences may result in more accurate nowcasts for the majority of the competitor models. While the MLP works best with 8 long sequences in every nowcasting scenario, other competitors yield better accuracy with 18 long input sequences in some nowcasting scenarios. This pattern is particularly visible for the different RNNs, where 8 long sequences work best in the 2-month nowcasting scenario while 18 long sequences yield better accuracy in the 1-month and 3-month

scenarios. The 1D CNN also generates its lowest RMSE and MAE values with 18 long input sequences, concretely in the 3-month nowcasting scenario. Seeing this all together, we can say that longer input sequences can improve the competitors' nowcasting performance during the first evaluation period. However, this effect ceases above a relatively low threshold of around 18 months (6 quarters). With 8 long input sequences in the 2-month nowcasting scenario, the GRU generates a relative RMSE of 0.562 and a relative MAE of 0.627, beating the benchmark model on a 5% significance level. With these results, the GRU achieves the best accuracy among the competitor models during the first evaluation period, Figure 9a below plots the nowcasts generated by the best-performing GRU configuration against the actual GDP growth during the first evaluation period. Then Figure 9b shows the series of the nowcast errors and how the cumulative sum of the squared nowcast errors evolved relative to the benchmark model.

Regarding the competitor models' nowcasting performance across the different nowcasting scenarios, the additional informational content of the second-month data releases often results in significantly more accurate nowcasts. Comparing the 3-month and the 2-month nowcasting scenarios, we see that although additional informational content of the third-monthly data releases can improve the absolute accuracy of the nowcasts, the performance gain relative to the naive benchmark model does not change in terms of statistical significance.



(a) The actual quarterly GDP growth (y_q) versus the nowcasts generated by the best-performing competitor model ($\hat{y}_{c,q}$). Best accuracy is achieved by the GRU, with 8 long input sequences ($l = 8$) in the 2-month nowcasting scenario ($v = 3t - 1$). The evaluation period ranges from 2012:Q1 to 2019:Q4.



(b) Nowcast errors ($\hat{e}_{c,q} = y_q - \hat{y}_{c,q}$, left axis) and the relative cumulative sum of squared nowcast errors (RCSSE) for the best-performing competitor model. The RCSSE (right axis) is computed as $RCSSE_c = \sum_q \hat{e}_{c,q}^2 / \sum_q \hat{e}_{b,q}^2$, where $\hat{e}_{c,q}^2$ denotes the squared nowcast error of the competitor model.

Figure 9: Nowcasting performance of the best-performing competitor model (GRU, $l = 8, v = 3t - 1$) during the first evaluation period. Source: Own editing based on FRED-MD.

After we have seen the results for the first evaluation period, Table 3 below reports the outcome of the empirical analysis for the second evaluation period which ranges from 2012:Q1 to 2022:Q4.

Table 3: Nowcasting performance of the competitor models relative to a naive constant growth model for GDP: RMSE and MAE evaluation. Evaluation period: 2012:Q1 – 2022:Q4.

	$v = 3t - 2$		$v = 3t - 1$		$v = 3t$	
	RMSE	MAE	RMSE	MAE	RMSE	MAE
MLP ($l = 8$)	0.351	0.471*	0.389	0.467*	0.354	0.436**
MLP ($l = 18$)	0.444	0.561*	0.470	0.553*	0.417	0.556*
MLP ($l = 36$)	0.482	0.601*	0.512	0.599*	0.492	0.603*
MLP ($l = 48$)	0.524	0.633*	0.524	0.611*	0.507	0.599*
1D CNN ($l = 8$)	0.482	0.528*	0.405	0.493*	<u>0.185*</u>	<u>0.338**</u>
1D CNN ($l = 18$)	0.550	0.606*	0.465	0.526*	0.226*	0.389**
1D CNN ($l = 36$)	0.642	0.669*	0.575	0.630*	0.462	0.616*
1D CNN ($l = 48$)	0.632	0.676*	0.591	0.617*	0.467	0.581*
RNN ($l = 8$)	0.251*	0.422**	0.235*	0.384**	0.392	0.487*
RNN ($l = 18$)	0.321	0.462**	0.203*	0.362**	0.448	0.526*
RNN ($l = 36$)	0.312*	0.480**	0.255*	0.404**	0.606	0.631*
RNN ($l = 48$)	0.286*	0.453**	0.242*	0.404**	0.562	0.601*
LSTM ($l = 8$)	0.433	0.539*	0.515	0.546*	0.605	0.638*
LSTM ($l = 18$)	0.451	0.548*	0.536	0.571*	0.577	0.598*
LSTM ($l = 36$)	0.505	0.595*	0.545	0.597*	0.604	0.62*
LSTM ($l = 48$)	0.504	0.582*	0.523	0.572*	0.625	0.625*
GRU ($l = 8$)	0.409	0.535**	0.521	0.551*	0.586	0.639*
GRU ($l = 18$)	0.422	0.536**	0.528	0.546**	0.564	0.591*
GRU ($l = 36$)	0.455	0.571**	0.531	0.576**	0.641	0.636*
GRU ($l = 48$)	0.427	0.554*	0.478	0.542**	0.642	0.646*

Notes: This table reports the relative RMSE and MAE of GDP growth for our competitor models relative to a naive constant growth model for GDP. A value below one indicates that the competitor model beats the naive benchmark model. The stars denote statistical significance at 10%(*), 5%(**) and 1%(***) level of the one-sided Diebold and Mariano (1995) test. Columns are related to the individual nowcasting scenarios: e.g. $v = 3t - 2$ refers to the 1-month nowcasting scenario. Within each nowcasting scenario, best (lowest) relative RMSE and MAE values are highlighted in bold for each competitor model. The overall best relative RMSE and MAE values are highlighted in bold and underlined.

Table 3 shows that all of the competitor models achieve better accuracy in terms of relative RMSE and MAE evaluation compared to what we have seen during the first evaluation period. Controversially though, we see a somewhat opposite picture regarding statistical significance: While we see much better (lower) relative RMSE values, none of the competitor models can beat the naive benchmark model on a 5% significance level. The reason for this counter-intuitive phenomenon can be traced back to the special characteristics of the evaluation period. The sharp

V-shaped recession in 2020:Q2 and Q3 is indicated by extreme values (*outliers*) in the target series. The naive benchmark model, which assumes constant growth, performs particularly badly in those periods, generating huge swings for the Diebold – Mariano loss differential as well. Recalling the formula of the Diebold and Mariano (1995) test statistic, these extreme values affect the variance of the loss differential (series) much more than its mean. Along with these considerations, we believe that the results in Table 3 provide some valuable insights into the generalization capabilities of the different competitor models and the role of long-term memory.

First, the MLP’s simple time-agnostic architecture performs much better than in the first evaluation period. Results in Table 3 clearly show that the best-performing configuration for the MLP is the one trained with the shortest input sequences ($l = 8$). With only 8 long input sequences, the MLP generates significantly more accurate nowcasts regarding MAE evaluation than the benchmark model. In the 3-month nowcasting scenario, when intra-quarterly data releases are available for all three months, the MLP yields a relative RMSE of 0.354 and a relative MAE of 0.436. This significant performance gain during the second evaluation period corresponds to the fact that the MLP detects the COVID crisis almost as well as the overall best-performing competitor model. While the MLP cannot beat the benchmark model significantly regarding RMSE evaluation, it generates more accurate nowcasts than the gated RNNs.

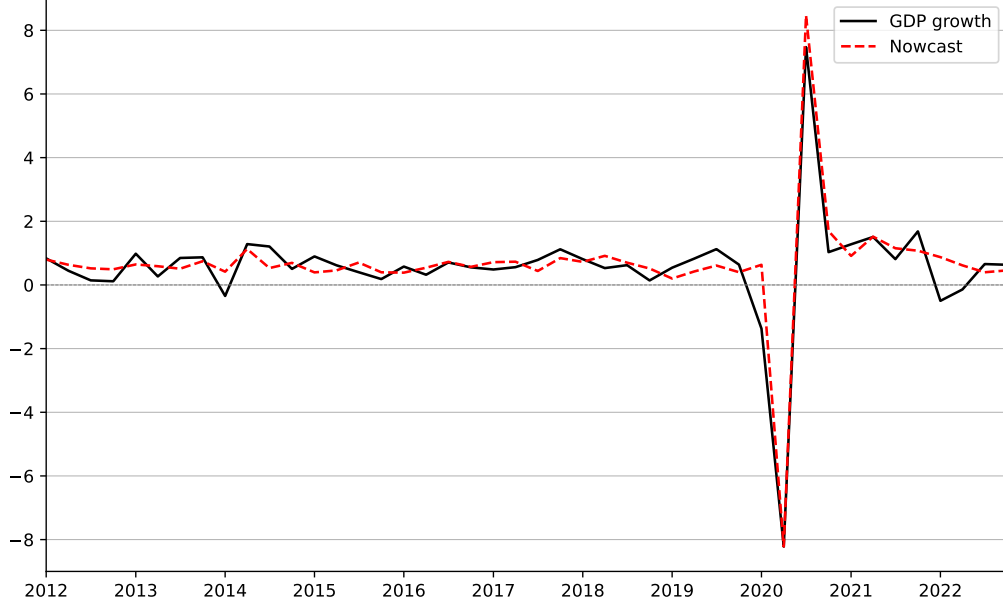
While the 1D CNN also achieved good accuracy during the first evaluation period, it performs even better here. Compared to the results from the first evaluation period, the 1D CNN favors the shorter input sequences during the second test period. The network performs best in all three nowcasting scenarios with 8 long input sequences. Furthermore, with 8 long input sequences in the 3-month nowcasting scenario, the 1D CNN generates a relative RMSE of 0.185 and a relative MAE of 0.338, yielding the overall best accuracy among the competitors during the second evaluation period. Figure 10a below plots the nowcasts generated by the best 1D CNN configuration ($l = 8, v = 3t$) against the actual growth. Then Figure 10b shows how the series of the nowcast errors and the cumulative nowcast errors have evolved during the second test period.

As we see in Table 3, the Elman RNN with 8 and 18 long input sequences generates similarly accurate nowcasts as the best MLP and 1D CNN configurations. Interestingly, the best results for the basic RNN are measured in the 1-month and 2-month scenarios, i.e., based on a relatively narrower information set. In the 1-month nowcasting scenario with 8 long input sequences, the basic RNN generates a relative RMSE of 0.251 and a relative MAE of 0.422. In the 2-month nowcasting scenario with 8 long input sequences, the basic RNN generates a relative RMSE of 0.203 and a relative MAE of 0.362. These values represent a significant performance advantage over the benchmark model, which applies to a 10% and 5% significance level, respectively. Furthermore, in these nowcasting scenarios, the Elman RNN achieves even better accuracy than the 1D CNN. In the 3-month nowcasting scenario, however, the basic RNN fails to beat the benchmark model significantly in terms of RMSE evaluation, falling short of the 1D CNN’s accuracy. Overall, results for the Elman network indicate strong nowcasting performance during the second test period. Table 3 also shows that the basic RNN produces clearly better nowcasts than its architecturally more advanced variants. Whereas the two gated RNNs generated equally

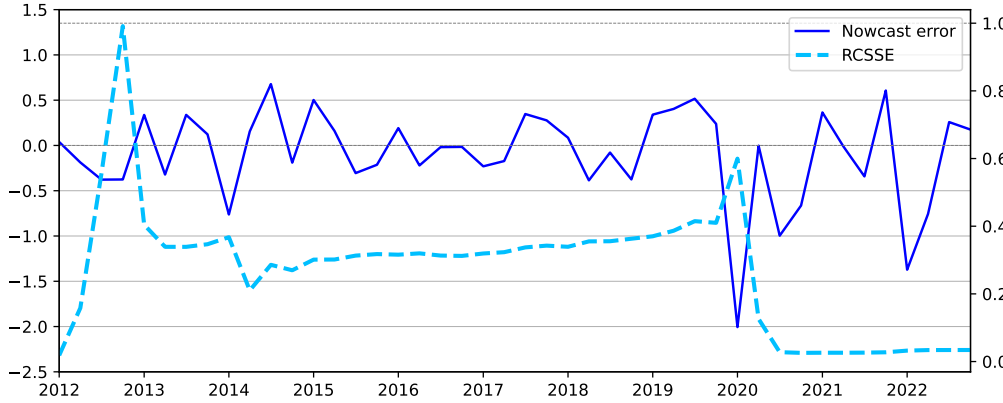
accurate (LSTM) or more accurate (GRU) nowcasts than the vanilla RNN during the first evaluation period, the basic Elman network shows significantly better generalization capability during the second evaluation period.

Table 3 shows that nowcasting accuracy generally weakens with longer input sequences for all competitor models. Results for the GRU, however, suggest that longer sequences could lead to better nowcasting performance for this specific network - at least in some nowcasting scenarios. This relationship is primarily noticeable in the 2-month nowcasting scenario, where accuracy slightly improves with longer input sequences. Above 18 months, however, the performance gain from the longer input sequences is not statistically significant over the benchmark model. It is also worth noting that the GRU's best accuracy is achieved in the 1-month nowcasting scenario when the network is trained with only 8-month-long sequences, generating a relative RMSE of 0.409 and a relative MAE of 0.535. As results in Table 3 signify, there is no training configuration for the GRU with which the network could generate significantly more accurate nowcasts than the benchmark in terms of RMSE evaluation. With input sequences longer than 48 months, nowcasting accuracy worsens considering both RMSE and MAE values for all competitor models.

Ultimately, the relatively weak performance of the gated RNNs suggests that long-term memory does not help predict sharp changes in economic growth, just like the V-shaped recession of 2020:Q2 and Q3. In general, architectural complexity and longer input sequences seem to hinder the detection of structural breaks and affect the competitor models' generalization capability badly during the second evaluation period.



(a) The actual quarterly GDP growth (y_q) versus the nowcasts generated by the best-performing competitor model ($\hat{y}_{c,q}$). Best accuracy is achieved by the 1D CNN, with 8 long input sequences ($l = 8$) in the 3-month nowcasting scenario ($v = 3t$). The evaluation period ranges from 2012:Q1 to 2022:Q4.



(b) Nowcast errors ($\hat{e}_{c,q} = y_q - \hat{y}_{c,q}$, left axis) and the relative cumulative sum of squared nowcast errors (RCSSE) for the best-performing competitor model. The RCSSE (right axis) is computed as $RCSSE_c = \sum_q \hat{e}_{c,q}^2 / \sum_q \hat{e}_{b,q}^2$, where $\hat{e}_{c,q}^2$ denotes the squared nowcast error of the competitor model.

Figure 10: Nowcasting performance of the best-performing competitor model (1D CNN, $l = 8$, $v = 3t$) during the second evaluation period. Source: Own editing based on FRED-MD.

As we proposed, the 1D CNN might represent a “sweet spot” in terms of architectural design between the simple time-agnostic MLP and the more complex (gated) recurrent networks. Based on the combined results of Table 2 and Table 3, the 1D CNN seems to be a very suitable ANN architecture for GDP nowcasting: It significantly outperforms the benchmark model in the first evaluation period while it generates the most accurate nowcasts for the second evaluation period.

5 Conclusion

Our study applies different ANN architectures to nowcast GDP growth for the US economy. The main research question of the paper is how the length of the training sequences affects the different networks’ nowcasting performance. Previously, we have seen the results from two distinctively different evaluation periods. The first (2012:Q1 – 2019:Q4) is characterized by balanced economic growth, while the second (2012:Q1 – 2022:Q4) also includes periods of the COVID-19 crisis. Empirical results show that all the investigated ANN architectures outperform the nowcasting accuracy of the naive (constant growth) benchmark model during both evaluation periods: They generate relative RMSE and MAE values lower than one across all training configurations. The performance advantage of the competitors is almost always statistically significant, at least based on one of the evaluation criteria, and generally strengthens in significance with consecutive intra-quarterly data releases.

During the first evaluation period, longer training sequences may result in more accurate nowcasts for the majority of the competitor models. This effect ceases above a relatively low threshold of 18 months, however. While the MLP works best with 8 long sequences in every nowcasting scenario, other competitors yield better accuracy with 18 long input sequences in some nowcasting scenarios. Training sequences longer than 18 months do not result in significantly more accurate nowcasts for any competitors. During the second evaluation period, where detecting the COVID-19 crisis (i.e., a structural break) is apparently decisive for nowcasting performance, all the competitor models work best with the shortest training sequences. Longer training sequences do not help the competitor models’ predictive performance. Instead, they seem to weaken their generalization capability.

Seeing the results from the two evaluation periods combined, we can argue that longer training sequences generally do not lead to significantly more accurate nowcasts. Consequently, architectural features enabling long-term memory may not play an important role in GDP nowcasting. Alternatively, they represent a bad trade-off for this specific predictive analysis in terms of complexity and generalization capability. On the other hand, the 1D CNN represents a “sweet spot” in terms of architectural complexity, showing consistently good nowcasting performance in both test periods. During the first evaluation period, it generates a relative RMSE of 0.624 and a relative MAE of 0.687 beating the benchmark model on a 5% significance level. During the second evaluation period, the 1D CNN achieves the overall best accuracy, producing a relative RMSE of 0.185 and a relative MAE of 0.338. Consequently, first in the literature, we propose the use of this specific neural network architecture for GDP nowcasting.

Finally, we should emphasize that the paper presents the results for different behavioral models and not for an exact system identification procedure, where we know the underlying data-generating process. Accordingly, empirical results mainly speak about the different ANN architectures’ compatibility with this predictive analysis rather than the characteristics of GDP growth as a time series. Nonetheless, results of the empirical analysis suggest that long-term memory may not play an important role in GDP nowcasting.

Acknowledgements

We would like to thank Róbert Lieli, professor at the Central European University, for his invaluable feedback and support. He has helped and inspired our work in many ways.

References

- Amari, S.-i., Murata, N., Muller, K.-R., Finke, M., & Yang, H. H. (1997). Asymptotic statistical theory of overtraining and cross-validation. *IEEE transactions on neural networks*, 8(5), 985–996.
- Chernis, T., & Sekkel, R. (2017). A dynamic factor model for nowcasting canadian gdp growth. *Empirical Economics*, 53(1), 217–234.
- Chung, J., Gulcehre, C., Cho, K., & Bengio, Y. (2014). Empirical evaluation of gated recurrent neural networks on sequence modeling. *arXiv preprint arXiv:1412.3555*.
- Dematos, G., Boyd, M. S., Kermanshahi, B., Kohzadi, N., & Kaastra, I. (1996). Feedforward versus recurrent neural networks for forecasting monthly japanese yen exchange rates. *Financial Engineering and the Japanese Markets*, 3(1), 59–75.
- Diebold, F. X., & Mariano, R. S. (1995). Comparing predictive accuracy. *Journal of Business & Economic Statistics*, 253–263.
- Doz, C., Giannone, D., & Reichlin, L. (2011). A two-step estimator for large approximate dynamic factor models based on kalman filtering. *Journal of Econometrics*, 164(1), 188–205.
- Ekman, M. (2021). *Learning deep learning: Theory and practice of neural networks, computer vision, nlp, and transformers using tensorflow*. Addison-Wesley Professional.
- Elman, J. L. (1990). Finding structure in time. *Cognitive science*, 14(2), 179–211.
- Ganesh, P. (2019). Types of convolution kernels: Simplified. <https://towardsdatascience.com/types-of-convolution-kernels-simplified-f040cb307c37>
- Giannone, D., Reichlin, L., & Small, D. (2008). Nowcasting: The real-time informational content of macroeconomic data. *Journal of monetary economics*, 55(4), 665–676.
- Goodfellow, I., Bengio, Y., & Courville, A. (2016). *Deep learning* [http://www.deeplearningbook.org]. MIT Press.
- Greene, W. H. (2017). *Econometric analysis* (Third). Pearson Education.
- Heravi, S., Osborn, D. R., & Birchenhall, C. (2004). Linear versus neural network forecasts for european industrial production series. *International Journal of Forecasting*, 20(3), 435–446.
- Hochreiter, S., & Schmidhuber, J. (1997). Long short-term memory. *Neural computation*, 9(8), 1735–1780.
- Hodrick, R. J., & Prescott, E. C. (1997). Postwar u.s. business cycles: An empirical investigation. *Journal of Money, Credit and Banking*, 29, 1–16. <https://api.semanticscholar.org/CorpusID:154995815>

- Hopp, D. (2021). Economic nowcasting with long short-term memory artificial neural networks (lstm). *arXiv preprint arXiv:2106.08901*.
- Jiang, Y., He, Y., & Zhang, H. (2016). Variable selection with prior information for generalized linear models via the prior lasso method. *Journal of the American Statistical Association*, *111*(513), 355–376.
- Kiranyaz, S., Avci, O., Abdeljaber, O., Ince, T., Gabbouj, M., & Inman, D. J. (2021). 1d convolutional neural networks and applications: A survey. *Mechanical systems and signal processing*, *151*, 107398.
- Kourentzes, N., Barrow, D. K., & Crone, S. F. (2014). Neural network ensemble operators for time series forecasting. *Expert Systems with Applications*, *41*(9), 4235–4244.
- Kuan, C.-M., & Liu, T. (1995). Forecasting exchange rates using feedforward and recurrent neural networks. *Journal of applied econometrics*, *10*(4), 347–364.
- Loermann, J., & Maas, B. (2019). Nowcasting us gdp with artificial neural networks.
- Marcellino, M., & Schumacher, C. (2010). Factor midas for nowcasting and forecasting with ragged-edge data: A model comparison for german gdp. *Oxford Bulletin of Economics and Statistics*, *72*(4), 518–550.
- Matheson, T. D. (2014). New indicators for tracking growth in real time. *OECD Journal: Journal of Business Cycle Measurement and Analysis*, *2013*(2), 51–71.
- McCracken, M. W., & Ng, S. (2016). Fred-md: A monthly database for macroeconomic research. *Journal of Business & Economic Statistics*, *34*(4), 574–589.
- Olah, C. (2015). Understanding lstm networks. <http://colah.github.io/posts/2015-08-Understanding-LSTMs/>
- Stock, J. H., & Watson, M. W. (2002). Forecasting using principal components from a large number of predictors. *Journal of the American statistical association*, *97*(460), 1167–1179.
- Tkacz, G. (2001). Neural network forecasting of canadian gdp growth. *International Journal of Forecasting*, *17*(1), 57–69.
- Torres, D. G., & Qiu, H. (2018). Applying recurrent neural networks for multivariate time series forecasting of volatile financial data. *KTH Royal Institute of Technology: Stockholm, Sweden*.
- Wallis, K. F. (1986). Forecasting with an econometric model: The ‘ragged edge’ problem. *Journal of Forecasting*, *5*(1), 1–13.
- Werbos, P. J. (1990). Backpropagation through time: What it does and how to do it. *Proceedings of the IEEE*, *78*(10), 1550–1560.

A Data appendix

The TCODE column denotes the following data transformation for a series x :

1. No transformation
2. Δx_t
3. $\Delta^2 x_t$
4. $\log(x_t)$
5. $\Delta \log(x_t)$
6. $\Delta^2 \log(x_t)$
7. $\Delta \left(\frac{x_t - x_{t-1}}{x_{t-1}} \right)$

The FRED column gives mnemonics in FRED followed by a short description. Some series require adjustments to the raw data available in FRED. These variables are tagged by an asterisk to indicate that they have been adjusted and thus differ from the series from the source. For a detailed summary of the adjustments see McCracken and Ng (2016).

Group 1: Output and income

	ID	tcode	FRED	Description
1	1	5	RPI	Real Personal Income
2	2	5	W875RX1	Real personal income ex transfer receipts
3	6	5	INDPRO	IP Index
4	7	5	IPFPNSS	IP: Financial Products and Nonindustrial Supplies
5	8	5	IPFINAL	IP: Final Products (Market Group)
6	9	5	IPCONGD	IP: Consumer Goods
7	10	5	IPDCONGD	IP: Durable Consumer Goods
8	11	5	IPNCONGD	IP: Nondurable Consumer Goods
9	12	5	IPBUSEQ	IP: Business Equipment
10	13	5	IPMAT	IP: Materials
11	14	5	IPDMAT	IP: Durable Materials
12	15	5	IPNMAT	IP: Nondurable Materials
13	16	5	IPMANSICS	IP: Manufacturing (SIC)
14	17	5	IPB51222s	IP: Residential Utilities
15	18	5	IPFUELS	IP: Fuels
16	19	1	NAPMPI	ISM Manufacturing: Production Index
17	20	2	CUMFNS	Capacity Utilization: Manufacturing

Group 2: Labor market

ID	tcode	FRED	Description	
1	21*	2	HWI	Help-Wanted Index for United States
2	22*	2	HWIURATIO	Ratio of Help Wanted/No. Unemployed
3	23	5	CLF160OV	Civilian Labor Force
4	24	5	CE160V	Civilian Employment
5	25	2	UNRATE	Civilian Unemployment Rate
6	26	2	UEMPMEAN	Average Duration of Unemployment (Weeks)
7	27	5	UEMPLT5	Civilians Unemployed – Less Than 5 Weeks
8	28	5	UEMP5TO14	Civilians Unemployed for 5-14 Weeks
9	29	5	UEMP15OV	Civilians Unemployed – 15 Weeks and Over
10	30	5	UEMP15T26	Civilians Unemployed for 15 – 26 Weeks
11	31	5	UEMP27OV	Civilians Unemployed for 27 Weeks and Over
12	32*	5	CLAIMSx	Initial Claims
13	33	5	PAYEMS	All Employees: Total nonfarm
14	34	5	USGOOD	All Employees: Goods-Producing Industries
15	35	5	CES1021000001	All Employees: Mining and Logging: Industries
16	36	5	USCONS	All Employees: Construction
17	37	5	MANEMP	All Employees: Manufacturing
18	38	5	DMANEMP	All Employees: Durable Goods
19	39	5	NDMANEMP	All Employees: Nondurable Goods
20	40	5	SRVPRD	All Employees: Service-Providing Industries
21	41	5	USTPU	All Employees: Trade, Transportation and Utilities
22	42	5	USWTRADE	All Employees: Wholesale Trade
23	43	5	USTRADE	All Employees: Retail Trade
24	44	5	USFIRE	All Employees: Financial Activities
25	45	5	USGOVT	All Employees: Government
26	46	1	CES0600000007	Avg Weekly Hours: Goods-Producing
27	47	2	AWOTMAN	Avg Weekly Overtime Hours: Manufacturing
28	48	1	AWHMAN	Avg Weekly Hours: Manufacturing
29	49	1	NAPMEI	ISM Manufacturing: Employment Index
30	127	6	CES0600000008	Avg Hourly Earnings: Goods-Producing
31	128	6	CES2000000008	Avg Hourly Earnings: Construction
32	129	6	CES3000000008	Avg Hourly Earnings: Manufacturing

Group 3: Housing

ID	tcode	FRED	Description	
1	50	4	HOUST	Housing Starts: Total New Privately Owned
2	51	4	HOUSTNE	Housing Starts: Northeast
3	52	4	HOUSTMW	Housing Starts: Midwest
4	53	4	HOUSTS	Housing Starts: South
5	54	4	HOUSTW	Housing Starts: West
6	55	4	PERMIT	New Private Housing Permits (SAAR)
7	56	4	PERMITNE	New Private Housing Permits: Northeast (SAAR)
8	57	4	PERMITMW	New Private Housing Permits: Midwest (SAAR)
9	58	4	PERMITS	New Private Housing Permits: South (SAAR)
10	59	4	PERMITW	New Private Housing Permits: West (SAAR)

Group 4: Consumption, orders and inventories

ID	tcode	FRED	Description	
1	3	5	DPCERA3M086SBEA	Real personal consumption expenditures
2	4*	5	CMRMTSPLx	Real Manu. and Trade Industries Sales
3	5*	5	RETAILx	Retail and Food Services Sales
4	60	1	NAPM	ISM: PMI Composite Index
5	61	1	NAPMNOI	ISM: New Orders Index
6	62	1	NAPMSDI	ISM: Supplier Deliveries Index
7	63	1	NAPMII	ISM: Inventories Index
8	64	5	ACOGNO	New Orders for Consumer Goods
9	65*	5	AMDMNOx	New Orders for Durable Goods
10	66*	5	ANDENOx	New Orders for Nondefense Capital Goods
11	67*	5	AMDMUOx	Unfilled Orders for Durable Goods
12	68*	5	BUSINVx	Total Business Inventories
13	69*	2	ISRATIOx	Total Business: Inventories to Sales Ratio
14	130*	2	UMSCENTx	Consumer Sentiment Index

Group 5: Money and credit

ID	tcode	FRED	Description	
1	70	6	M1SL	M1 Money Stock
2	71	6	M2SL	M2 Money Stock
3	72	5	M2REAL	Real M2 Money Stock
4	73	6	AMBSL	St. Louis Adjusted Monetary Base
5	74	6	TOTRESNS	Total Reserves of Depository Institutions
6	75	7	NONBORRES	Reserves of Depository Institutions
7	76	6	BUSLOANS	Commercial and Industrial Loans
8	77	6	REALLN	Real Estate Loans at All Commercial Banks
9	78	6	NONREVSL	Total Nonrevolving Credit
10	79*	2	CONSPI	Nonrevolving consumer credit to Personal Income
11	131	6	MZMSL	MZM Money Stock
12	132	6	DTCOLNVHFNM	Consumer Motor Vehicle Loans Outstanding
13	133	6	DTCTHFNM	Total Consumer Loans and Leases Outstanding
14	134	6	INVEST	Securities in Bank Credit at All Commercial Banks

Group 6: Interest and exchange rates

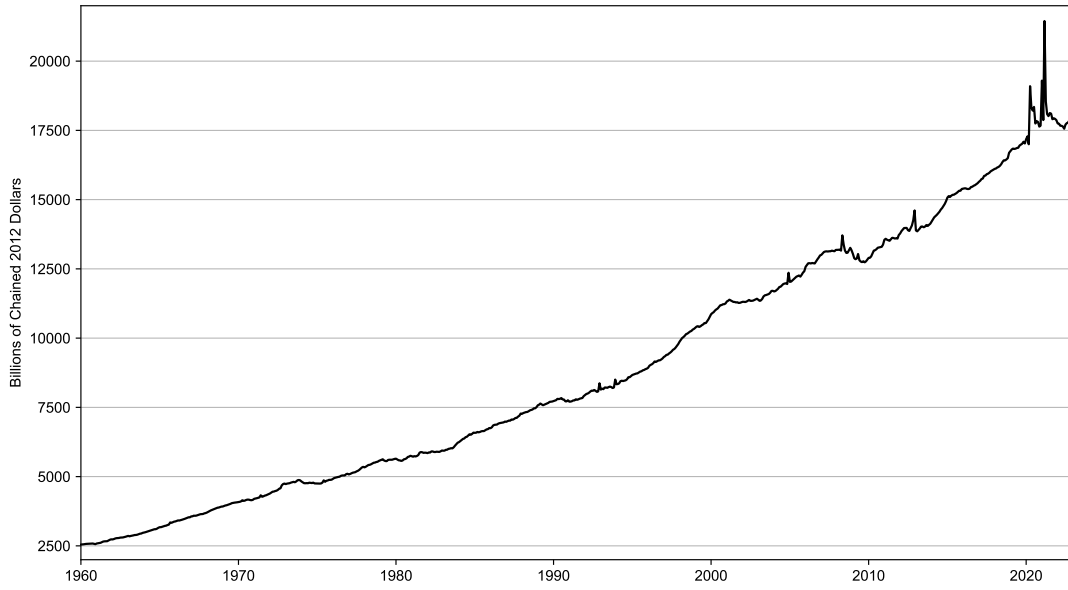
ID	tcode	FRED	Description
1	84	2	FEDFUNDS Effective Federal Funds Rate
2	85*	2	CP3Mx 3-Month AA Financial Commercial Paper Rate
3	86	2	TB3MS 3-Month Treasury Bill
4	87	2	TB6MS 6-Month Treasury Bill
5	88	2	GS1 1-Year Treasury Rate
6	89	2	GS5 5-Year Treasury Rate
7	90	2	GS10 10-Year Treasury Rate
8	91	2	AAA Moody's Seasoned Aaa Corporate Bond Yield
9	92	2	BAA Moody's Seasoned Baa Corporate Bond Yield
10	93*	1	COMPAPFFx 3-Month Commercial Paper Minus FEDFUNDS
11	94	1	TB3SMFFM 3-Month Treasury C Minus FEDFUNDS
12	95	1	TB6SMFFM 6-Month Treasury C Minus FEDFUNDS
13	96	1	T1YFFM 1-Year Treasury C Minus FEDFUNDS
14	97	1	T5YFFM 5-Year Treasury C Minus FEDFUNDS
15	98	1	T10YFFM 10-Year Treasury C Minus FEDFUNDS
16	99	1	AAAFFM Moody's Aaa Corporate Bond Minus FEDFUNDS
17	100	1	BAAFFM Moody's Baa Corporate Bond Minus FEDFUNDS
18	101	5	TWEXMMTH Trade Weighted U.S. Dollar Index: Major Currencies
19	102*	5	EXSZUSx Switzerland / U.S. Foreign Exchange Rate
20	103*	5	EXJPUSx Japan / U.S. Foreign Exchange Rate
21	104*	5	EXUSUKx U.S. / U.K. Foreign Exchange Rate
22	105*	5	EXCAUSx Canada / U.S. Foreign Exchange Rate

Group 7: Prices

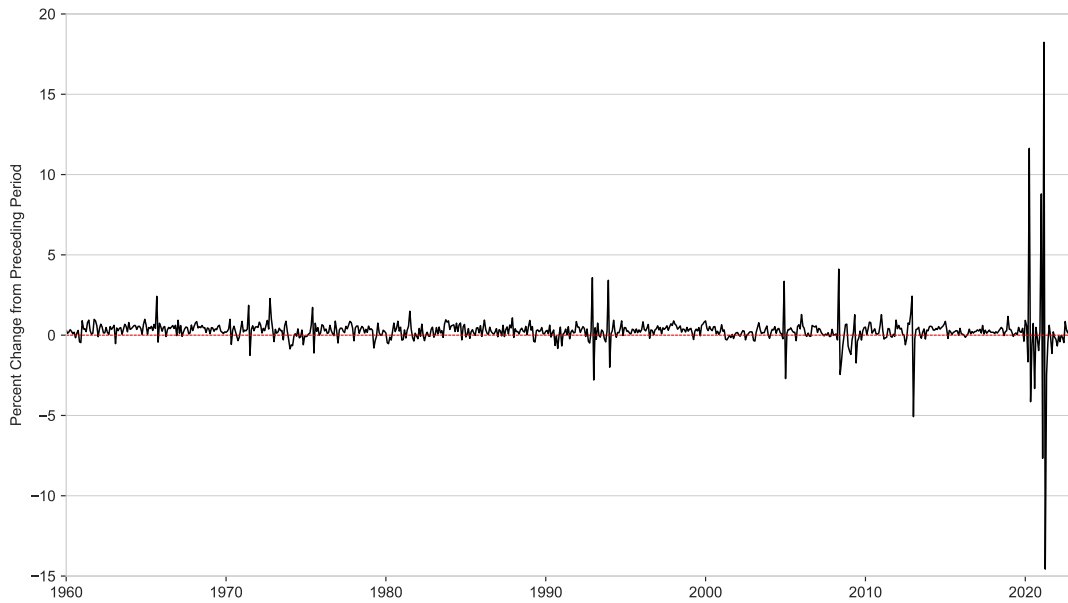
ID	tcode	FRED	Description	
1	106	6	WPSFD49207	PPI: Finished Goods
2	107	6	WPSFD49502	PPI: Finished Consumer Goods
3	108	6	WPSID61	PPI: Intermediate Materials
4	109	6	WPSID62	PPI: Crude Materials
5	110*	6	OILPRICE _x	Crude Oil, spliced WTI and Cushing
6	111	6	PPICMM	PPI: Metals and metal products
7	112	1	NAPMPRI	ISM Manufacturing: Prices Index
8	113	6	CPIAUCSL	CPI: All Items
9	114	6	CPIAPPSL	CPI: Apparel
10	115	6	CPITRNSL	CPI: Transportation
11	116	6	CPIMEDSL	CPI: Medical Care
12	117	6	CUSR0000SAC	CPI: Commodities
13	118	6	CUSR0000SAD	CPI: Durables
14	119	6	CUSR0000SAS	CPI: Service
15	120	6	CPIULFSL	CPI: All Items less Food
16	121	6	CUSR0000SA0L2	CPI: All Items less Shelter
17	122	6	CUSR0000SA0L5	CPI: All Items less Medical Care
18	123	6	PCEPI	Personal Cons. Expend.: Chain Index
19	124	6	DDURRG3M086SBEA	Personal Cons. Expend.: Durable Goods
20	125	6	DNDGRG3M086SBEA	Personal Cons. Expend.: Nondurable Goods
21	126	6	DSERRG3M086SBEA	Personal Cons. Expend.: Services

Group 8: Stock market

ID	tcode	FRED	Description	
1	80*	5	S&P 500	S&P's Common Stock Price Index: Composite
2	81*	5	S&P: indust	S&P's Common Stock Price Index: Industrials
3	82*	2	S&P div yield	S&P's Composite Common Stock: Dividend Yield
4	83*	5	S&P PE ratio	S&P's Composite Common Stock: Price-Earnings Ratio



(a) Real personal income (RPI): Original time series with trend.



(b) Real personal income (RPI): Log-differenced, detrended time series.

Figure A.1: Real personal income (RPI, $ID: 1$) before and after the corresponding data transformation ($tcode: 5$). Source: FRED-MD.